Isometric Spiracular Scaling in Scarab Beetles: Implications for Diffusive and Advective Oxygen Transport

Julian M. Wagner[1], C. Jaco Klok[1], Meghan E. Duell[1], John J. Socha[2], Guohua Cao[2], Hao Gong[2], Jon F. Harrison[1]

[1]*School of Life Sciences, Arizona State University, Tempe, AZ 85287-4501, USA*

[2]*Department of Biomedical Engineering and Mechanics, Virginia Tech, VA 24061, USA*

Short title: Spiracle scaling of beetles

Corresponding author: Jon Harrison, School of Life Sciences, Arizona State University, Tempe, AZ 85287-4501 USA, +1 (480)-965-9459; j.harrison@asu.edu

Abstract

The scaling of respiratory structures has been hypothesized to be a major driving factor in the evolution of many aspects of animal physiology. Here we provide the first assessment of the scaling of the spiracles in insects using ten scarab beetle species differing 180x in mass, including some of the most massive extant insect species. Using X-ray microtomography, we measured the cross-sectional area and depth of all eight spiracles, enabling the calculation of their diffusive and advective capacities. Each of these metrics scaled with geometric isometry. Because diffusive capacities scale with lower slopes than metabolic rates, the largest beetles measured require 10-fold higher PO_2 gradients across the spiracles to sustain metabolism by diffusion compared to the smallest species. Large beetles can exchange sufficient oxygen for resting metabolism by diffusion across the spiracles, but likely no scarab beetle can do so during flight. In contrast, spiracular advective capacities scale more steeply than metabolic rates, so larger beetles should require less pressure to drive sufficient ventilation to meet oxygen demands, assuming similar extraction efficiencies. These data illustrate a general principle of gas exchange: scaling of respiratory transport structures with geometric isometry diminishes the potential for diffusive gas exchange but enhances advective capacities; combining such structural scaling with muscle-driven ventilation allows larger animals to achieve high metabolic rates when active.

Keywords

Spiracle, scaling, Scarabaeidae, tracheal system, body size, oxygen transport

MAIN TEXT

Introduction

As animal species evolve different sizes, many aspects of their physiology and morphology scale disproportionately with one another (allometrically) with consequences for animal behavior, life history, evolution, and diversity (1-3). A driver of this disproportionality lies in the nonlinear scaling of geometry: doubling the radius of a sphere gives quadruple the surface area and octuple the volume; in a similar way, scaling up a small body plan gives drastically altered ratios of surface area, volume, and body length. Since the challenges associated with changes in body size have a geometric origin, they are ubiquitous. As a result, understanding the mechanisms animals use to overcome the effects of changes in geometric proportions remains a pervasive, important, and challenging biological problem. Three related aspects of animal function modulated by allometry are scaling of animal metabolic rates, generally scaling with $mass^{0.75}$ (4, 5), limits on the maximal body sizes of specific taxa (6, 7), and gas exchange strategies (8). For gas exchange, volume of tissue and hence potential gas exchange needs of animals scale with the cube of length (like the sphere), while surface areas tend to scale with the square of length. This leads to a decline in the ratio of surface area to volume with size. As a consequence, when animals evolve larger sizes, they may need to adapt the proportions of their respiratory structures or increase the use of advection (bulk flow) to avoid facing limitations based on processes that depend more on surface area such as diffusion.

Limitations on the capacity of larger animals to support oxygen delivery to tissues have been proposed to drive the hypometric scaling of metabolic rates with size, as well as the hypometric scaling of many physiological (e.g., heart and ventilation rates) and

behavioral/ecological traits (e.g., territory size, dispersal distance) (1-4, 9). However, competing theories suggest that other factors, such as heat dissipation constraints, nutrient uptake constraints, or performance-safety trade-offs, drive the hypometric scaling of metabolic rates and correlated variables, and that evolutionary adaptations of respiratory systems to size allow animals to match oxygen supply to need regardless of body size (10-13). One important step in resolving this controversy is determining how respiratory structures and mechanisms scale. The vast majority of prior studies of the scaling of gas exchange structures have focused on vertebrates, especially mammals. In contrast, there is relatively limited information on the scaling of gas exchange structures in invertebrates, despite the fact that most animal species are invertebrates (5, 14). The scaling of the insect respiratory system is of particular interest, as aspects of tracheal system structure have been reported to scale hypermetrically, in contrast to the isometric or hypometric scaling of respiratory structures in vertebrates, supporting the hypothesis that possession of a tracheal respiratory system limits insect body size (6, 15-18). Here, we report the first study of the scaling of insect spiracles, the gateway of air into the body and the first step in oxygen delivery from air to tissues, presenting new insight into a key morphological pathway in this most biodiverse clade of terrestrial animals.

Gas exchange usually occurs in a series of steps, often a sequence of alternating diffusive and advective processes. The capacity for a respiratory surface to conduct oxygen (diffusive conductance, G_{diff}) can be described using Fick's law, that is

$$(1)\ G_{diff} = \frac{\text{area}}{\text{thickness}} * K.$$

where K is Krogh's diffusion constant for oxygen in the barrier. The diffusive oxygen exchange across the surface (J_{diff}, mol sec^{-1}) is given by

65 (2) $J_{diff} = G_{diff} * \Delta P_{O2}$.

66 where ΔP_{O2} is the partial pressure gradient for oxygen across the exchanger. When gas exchange
67 relies on diffusion across a barrier, either G_{diff} or ΔP_{O2} must increase to match the increased
68 oxygen demand inherent in a larger body size (a larger relative tissue volume), or oxygen supply
69 will limit metabolic rate. Increases in G_{diff} may be accomplished by either a decrease in diffuser
70 thickness or increase in area. The ΔP_{O2} from air to mitochondria can be no greater than
71 atmospheric P_{O2} (approximately 21 kPa at sea level); this biophysical constraint sets an upper
72 limit on the ability of large animals to utilize increases in ΔP_{O2} to overcome a G_{diff} that does not
73 increase in proportion to oxygen consumption rate.

74 The scaling of surface area, barrier thickness, and ΔP_{O2} for gas exchangers across species
75 of animals varies with clade and developmental stage. In adult vertebrates, the scaling of the
76 passive diffusing capacity of the lung across species scales hypometrically, but matches the
77 scaling of metabolic rates (5). However, the scaling of respiratory morphology differs in
78 endotherms and ectotherms (5), as barrier thickness is constant with size in ectotherms, but
79 increases with size in endotherms. As a consequence, endotherms must scale surface area of the
80 lung more steeply than ectotherms to account for their increased barrier thickness and match the
81 scaling of G_{diff} to the scaling of metabolic rate. Bird eggs, which rely on diffusion through pores
82 for oxygen, employ a different strategy. Eggs of larger species have relatively thicker shells
83 (scaling with $mass^{0.45}$), increasing barrier thickness with size, likely to mitigate a higher
84 likelihood of mechanical damage (19). Pore area increases proportionally with shell thickness, so
85 G_{diff} per pore is relatively constant across egg size, and larger eggs have a higher density of pores
86 (20). The scaling of the G_{diff} of the shell overall matches the scaling of metabolic rate across

87 species, with both scaling hypometrically (19, 20). Pycnogonids (sea spiders) show yet another
88 pattern for the diffusing capacity of their respiratory structures (their legs). Unlike either bird
89 eggs or vertebrate lung membranes, pycnogonid barrier thickness scales isometrically (7). As in
90 bird eggs, there is an increase in the area-specific diffusing capacity of the leg cuticle of larger
91 pycnogonids, although the morphological basis remains unclear (7). However, the increases in
92 diffusive conductance of the respiratory exchanger are not sufficient to match increases in
93 metabolic rates with size, so the ΔP_{O2} across the leg cuticle increases in larger pycnogonid
94 species, which may limit maximal species size in this taxa (7).

95 Advective steps in gas exchange can occur using either air or fluid media and represent a
96 second broad strategy for delivering gases to tissues. The morphological capacity for a structure
97 to transport a fluid by advection can be described from Poiseulle's law,

98 (3) $G_{adv} = \frac{\text{area}^2}{8 * \text{dynamic viscosity} * \text{length}}$.

99 Given this relationship, the advective transport of oxygen through the structure is given by

100 (4) $G_{adv} * [O_2]$.

101 where $[O_2]$ is the concentration of O_2 in the fluid. Some examples in mammals illustrate how
102 morphology scales for structures relying on advection. In mammals, the radius of the aorta scales
103 with $\text{mass}^{0.375}$, and the length of the aorta scales with $\text{mass}^{0.25}$, suggesting that G_{adv} of the aorta
104 scales with $\text{mass}^{1.25}$ (4 * 0.375 – 0.25) (21). The tracheal-bronchial system is the advective
105 structure for air transport in vertebrates; radius scales with $\text{mass}^{0.39}$ while lengths scale with
106 $\text{mass}^{0.27}$, suggesting that G_{adv} for mammalian aorta and bronchial systems scale with $\text{mass}^{1.29}$
107 (22). G_{diff} for these same structures, on the other hand, scale as $\text{mass}^{0.5}$. Thus, the morphological
108 structures of mammalian respiratory systems seem to scale such that advective capacities

increase more than metabolic rates in larger species, while diffusive capacities decline. Of course, mammalian oxygen transport through the bronchial tree and circulatory system is thought to rely on advection regardless of size.

The design of the insect tracheal system is fundamentally different from either the vertebrate respiratory system or that of skin-breathing aquatic invertebrates; and it remains unclear how the components of the system scales. In insects, spiracles provide a (usually) gated opening to an air-filled conduit system that branches through the insect, with oxygen transported in the gas phase to the most distal surface of the tracheoles, with diffusion then occurring from tracheole to mitochondria (23). Since Krogh's demonstration that diffusion should suffice for oxygen transport in a relatively large Lepidopteran larvae, diffusion has been considered to be an important mechanism of gas exchange in insects (24, 25). However, many insects supplement diffusion with advection, especially when active (23, 26, 27). The spiracles are potentially an important step in insect gas exchange, since they are relatively small (difficult to see by eye in most insects) and yet must sustain all gas flux. It appears that spiracle morphology just matches gas exchange needs at peak metabolic performance with little additional capacity; for example, sealing of just one thoracic spiracle reduces flight metabolic rate in *Drosophila* (28). At present it is not clear whether the size of spiracles should best match G_{diff}, G_{adv} or some other physiological capacity. To shed light on this question, we used micro-computed tomography (micro-CT) (29) to provide the first interspecific examination of the scaling of spiracles, using ten species of scarab beetles spanning two orders of magnitude in mass, including some of the most massive extant species.

Methods

Acquisition of raw micro-CT images

132 Seventeen individuals of ten species (1-2 individuals per species) of scarab beetles (Fig.
133 1a) with a size range from 0.097 to 18 grams were obtained via breeders from online sources.
134 We examined the following species: *Goliathus goliathus*, *Coelorrhina hornimani*, *Dicronorrhina*
135 *derbyana*, *Mecynorrhina torquata*, *Eudicella euthalia*, *Protaetia orientalis*, *Popilia japonica*,
136 *Trypoxylus dichotomus*, *Dynastes hercules*, and *Cyclocephalis borealis*. Most species had both
137 male and females represented. Most specimens were scanned using a micro-CT scanner
138 (Skyscan 1172, Bruker, Bilerica, MA, USA) equipped with a Hammamatsu 1.3 MP camera and
139 Hammamatsu SkyScan Control software at Virginia Tech. To maintain tracheal structure in their
140 natural configuration, we used a minimal preparation of fresh samples (30). All beetles were
141 killed using ethyl acetate fumes, stored at 4 °C, and scanned within three days. They were
142 warmed back to room temperature to avoid motion artifacts from fluid flow, placed in X-ray
143 translucent polyimide tubing (Kapton, Dupont), and centered on a brass stage with putty. Power
144 was set at 10 W, voltage was adjusted for optimum brightness and contrast (70-96 kV), with
145 currents between 104-141 μA. Beetles were scanned with 0.4° rotation steps for 180° with frame
146 averaging. A flat-field correction was applied to all scans to account for subtract aberrations. All
147 raw projection images were collected a size of 1024 x 1280 pixels, yielding a scaling of 12-98
148 μm/pixel that was independent of beetle size. Average measured spiracle dimensions for
149 width/height/depth for the smallest beetles were around 10 pixels and hence resolvable with
150 minimally 10% resolution. Small beetles could be captured in a single scan, but larger beetles
151 were scanned sequentially in segments along their longitudinal axis by varying their position
152 relative to the beam.
153 *Dynastes hercules* were too large to be scanned with the same instrument, so these
154 beetles were imaged using an in-house-built bench-top micro-focus X-ray computed tomography

155 (micro-CT) platform (see (31, 32) for details) at Virginia Tech. The X-ray tube (Oxford
156 Instrument, Inc.) was operated at 70 kV and tube power was fixed at 20 W. Images were
157 collected with an X-ray flat-panel detector (model C7921, Hamamatsu, Inc.) operated at 1x1
158 binning mode, with a detector element size of 50 x 50 µm. The axial scanning field-of-view
159 (FOV) was 37.2 mm in diameter. In each scan, images were collected at 0.5° intervals as the
160 beetle was rotated through 360°, resulting in a total of 720 X-ray projections per scan. Because
161 the specimen was larger than the field of view, multiple scans were conducted sequentially along
162 the animal's anterior-posterior axis to image the entire body. The axial slice images were
163 reconstructed using the standard filtered back-projection (FBP) reconstruction algorithm, with an
164 image matrix of 1008 x 1012 px and an isotropic pixel size of 36.8 x 36.8 µm.

165 *Image Reconstruction and Measurements*

166 Raw micro-CT images were imported into NRecon reconstruction software from
167 SkyScan (Bruker, Bilerica, MA, USA). Ring artifact and beam hardening corrections were
168 applied where necessary, and contrast was optimized using the software's interactive histogram
169 feature. For large beetles that required multiple scans, reconstructions were set to align and fuse
170 automatically. Slices generated in NRecon were imported into Avizo 9 software (ThermoFisher
171 Scientific, Waltham, MA, USA) for 3D reconstructions.

172 Spiracles were identified by the characteristic slit-like shape of the opening, and the
173 bellows-shaped air sac behind it (Figure 1b, 1c, 1d). Spiracle locations were confirmed by
174 dissection on representative specimens. Measurements were taken for one of the paired six
175 abdominal and two thoracic spiracles for each beetle (Figure 1b,1c). A few scans had small
176 aberrant regions (e.g., blurriness) due to challenges in scanning, so which spiracle was measured
177 varied between the symmetric right and left side of an animal based on which region of the scan

178 was best resolved. Diameters of the spiracular opening were measured at the widest point of
179 opening to the outside air in the transverse and sagittal planes. Area of the opening was then
180 calculated assuming an elliptical shape, with the lengths of the semi-major/minor axes being the
181 diameters measured in the transverse and sagittal planes (Figure 1d). The depth of the spiracle
182 was measured from the outer opening to the interior valve connecting the spiracle to the tracheal
183 trunk (Figure 1d). The sex, mass and dimensions of all measured spiracles are provided in
184 supplementary tables 1 and 2.

185 *Calculations and Statistical Analyses*

186 We measured the scaling relationships for each spiracle separately, using log-log plots.
187 As dependent variables in these regressions, we tested $\log_{10}$ transformed spiracular depth, area,
188 area/depth (as an index of the diffusive capacity of the spiracle, see Eq. 1), and area^2/depth (as an
189 index of the resistance of the spiracle to advective flow, see Eq. 3 below).

190 We used two statistical approaches to assess the role of the phylogenetic relatedness of
191 the animals in scaling patterns: a phylogenetic generalized linear model (pGLS) and a generative
192 Bayesian model. We ran and plotted pGLS results in R (33-39). The goal of pGLS is to account
193 for non-independence of data points due to phylogenetic relatedness in construction of the linear
194 model, which requires a phylogeny of the study species (40). We spliced together such a
195 phylogeny from multiple published scarab phylogenies. The branch positions for beetle
196 subfamilies (Dynastinae, Rutelinae and Cetoniinae) were determined using Hunt et al. (41). The
197 branches within Dynastinae were placed in the tree using work from Rowland and Miller (42),
198 and the branches of Cetoniinae determined with two trees, one from Mico et al. (43, 44) and the
199 other Holm (43, 44). Four of the genera in this study were present in the tree for Coleoptera
200 constructed by Bocak et al. (45), which indicated the same branch places as our spliced tree,

201 providing some positive confirmation for this tree structure. Branch lengths were set to a value of
202 one because actual branch lengths are not known. Similar to pGLS, we built a Bayesian model
203 assuming that the data were generated by a multivariate normal distribution with the covariance
204 matrix given by the amount of shared ancestry between species (amount of shared branch
205 length). See supplemental methods for the details of the model, selection of priors, and python
206 code. Detailed information on the analysis is available at the website for the paper here:
207 https://julianmwagner.github.io/spiracle_scaling/ and at the corresponding repository
208 (https://github.com/julianmwagner/spiracle_scaling). Analyses indicated that the parameter
209 characterizing the degree of phylogenetic signal in our data (λ) was non-identifiable
210 (supplemental figures 1,2); this result means that our data does not inform this parameter and it
211 could take on any value from zero (no phylogenetic signal) to one (strong phylogenetic signal)
212 with similar probability. Hence, we opted to omit the use of phylogenetic covariance from our
213 models since 1) the total non-identifiability made selecting a single λ via maximum likelihood
214 for the frequentist pGLS dubious, and 2) including it added no explanatory value to our Bayesian
215 regression (parameter samples for λ were essentially straight from the prior). We instead used
216 nonparametric bootstrapping (10,000 bootstrap replicates with ordinary least squares regression
217 slopes/intercepts/residual standard deviation as the summary statistics) to obtain confidence
218 intervals for our slope and intercept values. Additionally, we performed a Bayesian linear
219 regression. Our model was a normal likelihood with mean given by a line with slope and
220 intercept parameters. To obtain parameter estimates, we sampled using the Stan implementation
221 of Hamiltonian Monte Carlo (cmdstanpy) in Python. See supplemental methods for the details of
222 the model, selection of priors, and Python code and at the paper website/repository listed above.
223 No data were excluded.

We defined isometric scaling as scaling as follows:

$mass^{0.67}$ for areas

$mass^{0.33}$ for area/depth

$mass^{1}$ for $area^{2}$/depth,

according to basic principles of geometric similarity (assuming mass is proportional to volume). We observed whether the 95% confidence interval given by bootstrapping/parameter samples for the slope of our measures of spiracle morphology overlapped with the isometric prediction. To produce any *p* values, we calculated the number of bootstrap replicates with test statistic at least as extreme as a particular value of interest, e.g. slope compared to isometry.

The diffusive capacity of a spiracle (G_{diff}, nmol sec^{-1} kPa^{-1}) at 25°C was calculated as:

(1) $G_{diff} = \frac{\text{area}}{\text{depth}} * D * \beta$

with D (the diffusivity constant for O_2 in air) = 0.178 cm^2 sec^{-1} (46) and β (the capacitance coefficient for oxygen in air) = 404 nmol cm^{-3} kPa^{-1} (47). For a diffusive system,

(2) Oxygen consumption rate (nmol s^{-1}) = $\Delta PO_2 * G_{diff}$,

with ΔPO_2 = the partial pressure gradient for oxygen across the spiracle (kPa). Advective capacity (G_{adv}, m^3 s^{-1}•kPa^{-1}) was calculated as:

(3) $G_{adv} = \frac{\text{area}^2}{8 * \text{dynamic viscosity} * \text{length}}$

assuming a dynamic viscosity of air of 1.86 x 10^{-8} kPa sec (46). To calculate total diffusive or advective capacity per beetle, the diffusive/advective capacity for all eight spiracles was summed and doubled (to obtain the total for both sides of the animal).

To calculate the ΔPO_2 across the spiracles needed to supply the beetle's total metabolic demand by diffusion, the metabolic rate for a quiescent beetle at a body temperature of 25 °C of

246 a given mass was estimated from (48) with the following equation: $\log_{10}$(metabolic rate (μW)) =
247 3.2 + 0.75•$\log_{10}$(mass (g)). Based on (49), the metabolic rate of small insects during flight is in
248 the range of 8x the resting value, whereas it is on the order of 32x resting metabolic rate in large
249 insects. Most scarab beetles are endothermic during flight, so flight metabolic rates of these
250 warm beetles could double with a 10 °C increase in thoracic temperature if the Q_{10} is 2, resulting
251 in a 64x total increase. Even this calculation may be a conservative estimate of hovering
252 metabolic rate, as oxygen consumption rose to 90x higher (compared to quiescent) in fig beetles
253 in one study (50), and maximal flight metabolic rates may be 1.25-2x higher than those reported
254 during hovering (51-54). Therefore, we conservatively estimated maximal aerobic metabolic rate
255 during flight as 90x those of quiescent beetles. The required PO_2 gradient across the spiracles to
256 support gas exchange by diffusion at rest and during flight was calculated by rearranging
257 equation 2 and performing unit conversions as follows:

258 $$(4)\ \Delta PO_2\ (\text{kPa}) = \left(\frac{\left(10^{3.20+0.75*\log_{10}(\text{mass (g)})}\mu\text{W}\right)\left(\frac{1\ \frac{\mu\text{J}}{\text{s}}}{1\ \mu\text{W}}\right)\left(\frac{\text{nL}}{20.7\ \mu\text{J}}\right)\left(\frac{1\ \text{nmol}}{24.5\ \text{nL}}\right)}{\left(\frac{\text{area}}{\text{depth}}\ (\text{cm})\right)\left(0.178\ \frac{\text{cm}^2}{\text{sec}}\right)\left(404\ \frac{\text{nmol}}{\text{cm}^3\text{kPa}}\right)} \right).$$

259 where conversion factors of 20.7 kJ/L and 24.5 mol/L were assumed for O_2 at 25 °C.

260 **Results**

261 All spiracles scaled with geometric isometry for area, depth, area/depth (which
262 corresponds to diffusive capacity), and area^2/depth (which corresponds to advective capacity)
263 (figure 2, supplemental figure 3-7). Some example regressions with confidence intervals for the
264 slopes are shown in figure 2, illustrating scaling isometry, the larger size of the mesothoracic
265 spiracle, and the tight size distribution of the more anterior spiracles as compared to the
266 posterior. The mesothoracic spiracle was much larger than any of the other spiracles, consistent

267 with the general trend of increasing spiracular area closer to the anterior of the animal
268 (supplemental figure 3). The area of the mesothoracic spiracles was approximately four times
269 larger than both the metathoracic spiracles, and abdominal spiracles 1-3, and abdominal spiracles
270 4-6 were approximately half the size of the more anterior abdominal spiracles (supplemental
271 figure 3). Not only were anterior spiracles larger than posterior, but they also had much lower
272 variability around the trend line within the species assayed in this study (figure 2a,b,c). In
273 comparison, the depth of the spiracles showed much less variability in tightness of the
274 distribution around the scaling trend lines (figure 2d,e,f).

275 As with individual spiracles, the combined diffusing capacity of all the spiracles scaled
276 isometrically (Fig. 3a). However, because this slope was less than the scaling exponent for
277 metabolic rate (slope of 0.75, shown as the repeated light grey background lines), the required
278 pO_2 gradient across spiracles necessary to supply oxygen by diffusion increased by an order of
279 magnitude from the small to the large scarabs (Fig. 3b). The advective capacity increased with a
280 positive slope that was greater than the scaling exponent for metabolic rate (slope of 0.75, light
281 grey lines) (Fig. 3c).

282 **Discussion**

283 Spiracles scaled with geometric isometry. Isometric scaling of diffusive capacities means
284 that diffusion becomes increasingly less able to meet oxygen demands in larger beetles, with the
285 required gradient for oxygen transport by diffusion through the spiracles increasing by an order
286 of magnitude over two orders of magnitude in body mass. Conversely, our data demonstrate that
287 the advective capacities of the spiracles scale more positively than do metabolic rates. This result
288 strongly suggests that, if insects switch from diffusive to advective gas transport, there is no

289 physical constraint associated with spiracular gas exchange that limits insect size and metabolic
290 rates.

291 It is important to note that geometric isometry does not occur universally for tracheal
292 structures, or consistently across clades. Comparing tenebrionid beetles inter-specifically, the leg
293 tracheae scale hypermetrically, but the head tracheae scale isometrically (6). Within a bumblebee
294 species, one spiracle scales isometrically (16). In the leg of growing locust (*Schistocerca*
295 *americana*), the diffusing capacity of the large longitudinal tracheae of the leg scales
296 hypometrically (17), whereas in a growing caterpillar (*Manduca sexta*), diameters of most
297 tracheae scale isometrically (55). Why different scaling patterns are observed in these different
298 cases is unclear; more in-depth analysis of the required gas transport and the mechanism of
299 transport are needed to evaluate the scaling of individual tracheal system structures.

300 Diffusive capacities of the spiracles scaled with $mass^{0.39}$, well below the scaling slope for
301 oxygen consumption rate (approximately 0.75); thus, diffusion across the spiracles becomes
302 more challenging for larger insects. The required O_2 gradient across the spiracles to supply the
303 metabolic demand by diffusion increases by approximately an order of magnitude from our
304 smallest to largest beetles, but the size effect on the required PO_2 gradient is less important than
305 the effect of activity. For quiescent beetles, the PO_2 gradients across the spiracles necessary for
306 diffusion are low (0.05-0.46 kPa depending on size). However, during endothermic flight, the
307 required PO_2 gradient across the spiracles increases from 5 to 41 kPa, which is impossible to
308 achieve because the maximum partial pressure of oxygen in air is only 21 kPa. Because the
309 distance required for oxygen diffusion from air to the flight muscle is much greater than the
310 distance through the spiracle, these data illustrate the impossibility of diffusion sustaining
311 oxygen consumption during flight in these beetles, regardless of size. With metabolic rates

312 scaling with $mass^{0.75}$ and spiracular depth with $mass^{0.33}$, spiracular area would need to scale with
313 $mass^{1.08}$ (0.75 + 0.33) to conserve the required PO_2 gradient to support diffusion across all insect
314 sizes.

315 By contrast, advective capacity scales with $mass^{1.1}$, much higher than the slope for the
316 metabolic rate, so oxygen delivery via advection becomes easier for larger beetles even as
317 diffusion becomes impossible. This effect might reflect a shift toward increasing reliance on
318 advection as scarab beetles increase in size; alternatively, this increasing advective capacity
319 relative to metabolic rate may allow larger beetles to require lower pressures to drive advection
320 through their spiracles, assuming no scaling of extraction efficiency.

321 We also observe much tighter distributions in the scaling pattern for the area of the large
322 anterior spiracles as compared to the smaller posterior ones. This result may suggest that the
323 large anterior spiracles are more constrained in their morphology, since they presumably provide
324 the gas exchange needed for metabolically demanding tissues like the flight muscle and brain.

325 There are some important caveats when interpreting our data. Insect spiracles are
326 morphologically complex structures. We made 3D measurements using tomographic imaging,
327 but analyzed air transport capacities by modeling the spiracle as a cylinder, which could over or
328 underestimate capacity depending on factors like valve position and the complex shape of the
329 spiracular atrium. Furthermore, our CT scans were conducted on sacrificed specimens; the
330 assessment of spiracles of living insects could offer insights not possible with static morphology.
331 For example, living insects might control the shape of the bellows-like atrium and valves in a
332 concerted way to promote air flow. As yet, we know little about how the tracheal system
333 structure and function might scale differently in different species. As an example of a fairly
334 dramatic difference in tracheal system function across beetle clades, some Cerambycid beetles

335 use draft inward ventilation through the mesothoracic spiracle during flight, whereas most scarab
336 beetles autoventilate the thorax using wing movements (56, 57). Dung beetle species vary
337 between exhaling nearly all to none of their air out the mesothoracic spiracles, with species from
338 more arid environments exhibiting more expiration via the mesothoracic spiracle (58). Multiple
339 beetle species collapse parts of their tracheal system to produce advective airflow, both in adults
340 and as pupae (59-61). Though it is unclear how respiration via tracheal collapse differs with size
341 and in different species, the prevalence of active breathing further highlights the need for
342 advective airflow for insect function. The phylogenetic, life history, and environmental
343 influences on tracheal system structure, function, and scaling seem likely to be a ripe area for
344 future research.

345 Our finding of isometric scaling of insect spiracles would appear to differ from reports
346 for tracheae of mammals, in which radius scales with mass$^{0.39}$ and lengths with mass$^{0.27}$ (62).
347 However, confidence limits from our study included these scaling slopes, suggesting that
348 respiratory scaling of tracheal morphology may be congruent across these disparate groups.
349 Tenney and Bartlett's study (62) had greater power, as it examined 43 species ranging over 5
350 orders of magnitude in body mass. However, it worth noting that they did not consider error in
351 their slope estimates, test for statistical differences in slopes between the radii and lengths, or
352 consider phylogeny, so the conclusion that mammalian tracheae scale non-isometrically (and
353 differently from insect spiracles) could benefit from rigorous comparative analysis.

354 *Conclusions*: Insect spiracles scale with geometric isometry in beetles, which means that
355 diffusive capacities increase much less than metabolic rates as body size increases, while
356 advective capacities increase more rapidly than do metabolic rates. These are general principles
357 of gas exchange that should apply to respiratory structures of any animal clade exhibiting

isometric scaling. Nonetheless, resting oxygen consumption rates of the largest beetles can likely be supplied by diffusion, allowing even very large insects to recover from any form of anoxia it might experience . In contrast, endothermic flight, and likely strong terrestrial locomotion, require a strong ventilatory system, especially in larger insects.

Authors' contributions

JW helped with study design, collected spiracle measurements from the micro-CT data, carried out statistical analyses, and drafted the manuscript and figures. JFH helped with study design, coordinated the study, and drafting the manuscript. CJK and JJS collected the micro-CT data; additionally, Dynastes data were collected in collaboration with HG and GC. MED helped develop methods for analysis of micro-CT data, and helped with phylogenetic correction analysis. JJS also helped draft the manuscript. All authors gave approval for publication.

Funding

This research was supported in part by funds from the School of Life Sciences Undergraduate Research (SOLUR) Program through the School of Life Sciences at Arizona State University, Tempe Campus, and by NSF IOS 1122157 and 1558052.

References

1. Bonner JT. Why size matters: from bacteria to blue whales. Princeton, N.J.: Princeton University Press; 2006.
2. West GB. Scale: The Universal Laws of Growth, Innovation, Sustainability, and the Pace of Life in Organisms, Cities, Economics, and Companies. New York: Penguin Press; 2017.
3. Sibly RM, Brown JH, Kodric-Brown A. Metabolic Ecology: A Scaling Approach: Wiley-Blackwell; 2012.
4. West GB, Brown JH, Enquist BJ. A general model for the origin of allometric scaling laws in biology. Science. 1997;274:122-6.
5. Gillooly JF, Gomez JP, Mavrodiev EV, Rong Y, McLamore ES. Body mass scaling of passive oxygen diffusion in endotherms and ectotherms. Proceedings of the National Academy of Sciences. 2016;113(19):5340-5.
6. Kaiser A, Klok CJ, Socha JJ, Lee W-K, Quinlan MC, Harrison JF. Increase in tracheal investment with beetle size supports hypothesis of oxygen limitation on insect gigantism. Proceedings of the National Academy of Sciences. 2007;104(32):13198-203.
7. Lane SJ, Shishido CM, Moran AL, Tobalske BW, Arango CP, Woods HA. Upper limits to body size imposed by respiratory–structural trade-offs in Antarctic pycnogonids. Proceedings of the Royal Society B: Biological Sciences. 2017;284(1865).
8. Perry SF, Lambertz M, Schmitz A. Respiratory Biology of Animals. Evolutionary and Functional Morphology. Oxford, U.K.: Oxford Press; 2019.
9. Banavar JR, Moses ME, Brown JH, Damuth J, Rinaldo A, Sibly RM, et al. A general basis for quarter-power scaling in animals. Proceedings of the National Academy of Sciences. 2010;107(36):15816-20.
10. Glazier DS. Metabolic scaling in complex living systems. Systems. 2014;2(4):451-540.
11. Harrison JF. Do performance-safety trade-offs cause hypometric metabolic scaling in animals? Trends Ecol Evol. 2017;32(9):653-64.
12. Harrison JF. Approaches for testing hypotheses for the hypometric scaling of aerobic metabolic rate in animals. American Journal of Physiology-Regulatory, Integrative and Comparative Physiology. 2018;315(5):R879-R94.
13. White CR, Kearney MR. Metabolic scaling in animals: methods, empirical results, and theoretical explanations. Comprehensive Physiology. 2014;4:231-56.
14. Peters RH. The Ecological Implications of Body Size. Cambridge: Cambridge University Press; 1983.
15. Harrison JF, Kaiser A, VandenBrooks JM. Atmospheric oxygen level and the evolution of insect body size. Proceedings of the Royal Society B-Biological Sciences. 2010;277(1690):1937-46.
16. Vogt JF, Dillon ME. Allometric scaling of tracheal morphology among bumblebee sisters (Apidae: *Bombus*): compensation for oxygen limitation at large body sizes? Physiol Biochem Zool. 2013;86.
17. Harrison JF, Lafreniere JJ, Greenlee KJ. Ontogeny of tracheal dimensions and gas exchange capacities in the grasshopper, Schistocerca americana. Comparative Biochemistry and Physiology a-Molecular & Integrative Physiology. 2005;141(4):372-80.
18. Greenlee KJ, Henry JR, Kirkton SD, Westneat MW, Fezzaa K, Lee WK, et al. Synchrotron imaging of the grasshopper tracheal system: morphological components of tracheal hypermetry and the effect of age and stage on abdominal air sac volumes and convection.

American Journal of Physiology: Comparative, Regulatory and Integrative Physiology. 2009;297:1343-50.
19. Ar A, Rahn H. Pores in avian eggshells: gas conductance, gas exchange and embryonic growth rate. Respir Physiol. 1985;61(1):1-20.
20. Toien O, Paganelli CV, Rahn H, Johnson RR. Diffusive resistance of avian eggshell pores. Respir Physiol. 1988;74:345-54.
21. Holt JP, Rhode EA, Holt WW, Kines H. Geometric similarity of aorta, venae cavae, and certain of their branches in mammals. Am J Physiol. 1981;241:100-4.
22. Stahl WR. Scaling of respiratory variables in mammals. J Appl Physiol. 1967;22(3):453-60.
23. Harrison JF, Wasserthal LT, Chapman RF. Gaseous exchange. In: Simpson SJ, Douglas AE, editors. The Insects: Structure and Function. 5th ed. New York: Cambridge University Press; 2013. p. 501-45.
24. Krogh A. Studien über Tracheenrespiration. II. über Gasdiffusion in den Tracheen. Pflügers Archiv. 1920;179:95-112.
25. Hetz SK, Bradley TJ. Insects breathe discontinuously to avoid oxygen toxicity. Nature. 2005;433(7025):516-9.
26. Socha JJ, Forster TD, Greenlee KJ. Issues of convection in insect respiration: Insights from synchotron X-ray imaging and beyond. Respir Physiol Neurobiol. 2010;173S:S65-S73.
27. Wasserthal LT, Cloetens P, Fink RH, Wasserthal LK. X-ray computed tomography study of the flight-adapted tracheal system in the blowfly *Calliphora vicina*, analysing the ventilation mechanism and flow-directing valves. J Exp Biol. 2018;221:1-12.
28. Heymann N, Lehmann F-O. The significance of spiracle conductance and spatial arrangement for flight muscle function and aerodynamic performance in flying *Drosophila*. J Exp Biol. 2006;209(9):1662-77.
29. Iwan D, Kamiński MJ, Raś M. The Last Breath: A µCT-based method for investigating the tracheal system in Hexapoda. Arthropod Struct Dev. 2015;44(3):218-27.
30. Socha JJ, DeCarlo F. Use of synchrotron tomography to image naturalistic anatomy in insects. SPIE 2008;2008(Developments in X-Ray Tomography VI: San Diego, CA, USA):70780A-7.
31. Sharma KS, Gong H, Ghasemalizadeh O, Yu H, Wang G, Cao G. Interior micro-CT with an offset detector. Medical Physics. 2014;41(6):061915.
32. Gong H LJ, Zhou O, & Cao G Medical Imaging 2015: Physics of Medical Imaging, (International Society for Optics and Photonics), p 94124N, editor Implementation of interior micro-CT on a carbon nanotube dynamic micro-CT scanner for lower radiation dose. SPIE Medical Imaging; 2015.
33. Garnier S. Paxkage 'viridis' 2016 [Available from: https://cran.microsoft.com/snapshot/2016-08-05/web/packages/viridis/viridis.pdf.
34. Orme D. The caper package: comparative analysis of phylogenetics and evolution in R 2018 [Available from: https://cran.r-project.org/web/packages/caper/vignettes/caper.pdf.
35. Pinheiro J, Bates D, DebRoy Sa, Sarkar D, Team RC. Linear and Nonlinear Mixed Effects Models 2021 [Available from: {https://CRAN.R-project.org/package=nlme}.
36. Harmon LJ, Weir JT, Brock CD, Glor RE, Challenger W. GEIGER: investigating evolutionary radiations. Bioinformatics. 2008;24.
37. Revell LJ. phytools: an R package for phylogenetic comparative biology (and other things). Methods Ecol Evol. 2012;3.

38. Paradis E, Claude J, Strimmer K. APE: Analyses of Phylogenetics and Evolution in R language. Bioinformatics. 2004;20(2):289-90.
39. R-Core-Team. R: A language and environment for statistical computing Vienna, Austria: R Foundation for Statistical Computing; 2016 [Available from: http://www.R-project.org/.
40. R. P. Freckleton, P. H. Harvey, M. Pagel. Phylogenetic Analysis and Comparative Data: A Test and Review of Evidence. The American Naturalist. 2002;160(6):712-26.
41. Hunt T, Bergsten J, Levkanicova Z, Papadopoulou A, John OS, Wild R, et al. A comprehensive phylogeny of beetles reveals the evolutionary origins of a superradiation. Science. 2007;318(5858):1913-6.
42. Rowland JM, Miller KB. Phylogeny and systematics of the giant rhinoceros beetles (Scarabaeidae: Dynastini). Insecta Mundi 2012;0258-0263:1-15.
43. Holm E. On the genera of African Cetoniinae: Anisorrhina Westwood 1842, Melinesthes Kraatz 1880 and Inhambane Péringuey 1907. Tropical Zoology. 1993;6(1):165-77.
44. Micó E, Morón MA, Šípek P, Galante E. Larval morphology enhances phylogenetic reconstruction in Cetoniidae (Coleoptera: Scarabaeoidea) and allows the interpretation of the evolution of larval feeding habits. Syst Entomol. 2008;33(1):128-44.
45. Bocak L, Barton C, Crampton-Platt A, Chesters D, Ahrens D, Vogler AP. Building the Coleoptera tree-of-life for >8000 species: composition of public DNA data and fit with Linnaean classification. Syst Entomol. 2014;39(1):97-110.
46. Lide DR, editor. CRC Handbook of Chemistry and Physics. 72 ed. Boca Raton: CRC Press; 1991.
47. Piiper J, Dejours P, Haab P, Rahn H. Concepts and basic quantities in gas exchange physiology. Respir Physiol. 1971;13:292-304.
48. Chown SL, Marais E, Terblanche JS, Klok CJ, Lighton JRB, Blackburn TM. Scaling of insect metabolic rate is inconsistent with the nutrient supply network model. Funct Ecol. 2007;21:282-90.
49. Niven JE, Scharlemann JPW. Do insect metabolic rates at rest and during flight scale with body mass? Biol Lett. 2005;1:346-9.
50. Chappell MA. Thermoregulation and energetics of the green fig beetle *Cotinus texana* during flight and foraging behaviour. Physiol Zool. 1984;57:581-9.
51. Roberts SP, Harrison JF, Dudley R. Allometry of kinematics and energetics in carpenter bees (*Xylocopa* varipuncta) hovering in variable-density gases. J Exp Biol. 2004;207(6):993-1004.
52. Heinrich B. Thermoregulation in bumblebees II. Energetics of warm-up and free flight. Journal of Comparative Physiology. 1975;96:155-66.
53. Wolf TJ, Schmid-Hempel P, Ellington CP, Stevenson RD. Physiological correlates of foraging efforts in honey-bees: oxygen consumption and nectar load. Funct Ecol. 1989;3:417-24.
54. Lehmann FO, Dickinson MH. The changes in power requirements and muscle efficiency during elevated force production in the fruit fly Drosophila melanogaster. J Exp Biol. 1997;200(7):1133-43.
55. Lundquist TA, Kittilson JD, Ahsan R, Greenlee KJ. The effect of within-instar development on tracheal diameter and hypoxia-inducible factors α and β in the tobacco hornworm, Manduca sexta. J Insect Physiol. 2018;106:199-208.
56. Miller PL. The supply of oxygen to the active flight muscles of some large beetles. J Exp Biol. 1966;45:285-304.

509 57. Amos WB, Miller PL. The supply of oxygen to the active flight muscles of Petrognathus
510 gigas (F.) (Cerambycidae). Entomologist. 1965;98:88-94.
511 58. Duncan FD, Byrne MJ. The role of the mesothoracic spiracles in respiration in flighted
512 and flightless dung beetles. J Exp Biol. 2005;208(5):907-14.
513 59. Pendar H, Kenny MC, Socha JJ. Tracheal compression in pupae of the beetle Zophobas
514 morio. Biol Lett. 2015;11(6):20150259-.
515 60. Socha JJ, Lee W-K, Harrison JF, Waters JS, Fezzaa K, Westneat MW. Correlated
516 patterns of tracheal compression and convective gas exchange in a carabid beetle. J Exp Biol.
517 2008;211(21):3409-20.
518 61. Waters JS, Lee WK, Westneat MW, Socha JJ. Dynamics of tracheal compression in the
519 horned passalus beetle. American Journal of Physiology: Regulatory, Integrative and
520 Comparative Physiology. 2013;304:R621-R7.
521 62. Tenney SM, Bartlett D. Comparative quantitative morphology of the mammalian lung:
522 Trachea. Respir Physiol. 1967;3(2):130-5.

523

524 **Figure Legends**

525 Figure 1. Scarab beetles include large bodied individuals and have eight spiracles. (a)
526 Phylogenetic tree for the scarab beetles used in this study showing size distribution among clades
527 (branch lengths are meaningless). (b) Location of the eight spiracles in the scarab body. (c) 3D
528 reconstruction of the tracheal trunks in the thorax, legs and abdomen of *Dicronorrhina derbyana*;
529 spiracles are shown in white. The larger images of spiracles show the size of the opening (dark in
530 color) compared to the mushroom-shaped (white) atrium behind and the differences in spiracle
531 shape. (d) Transverse x-ray slice through the third abdominal spiracle with diameter, α, and
532 depth, β, measures illustrated.

533 Figure 2. Isometric scaling of scarab beetle spiracles. Spiracle area scales isometrically (A, B),
534 with much tighter distribution about the isometric model for the large anterior spiracles (e.g. the
535 mesothoracic spiracle as seen in A) as compared to the smaller posterior spiracles that may be
536 less critical for gas exchange to metabolically demanding tissues. C shows estimates for the
537 variability for regression models for the various spiracles (S mesothoracic, T metathoracic, 1-6
538 abdominal), calculated as the standard deviation divided by $10^{\text{regression intercept}}$, which represents the
539 spiracle area for a 1g beetle. Black diamond and line show the median and 2.5^{th}-97th residual
540 standard deviation divided by $10^{\text{regression intercept}}$ calculated on non-parametric bootstrap samples.
541 The white diamond and grey interval represent the median and 3rd-97th highest posterior density
542 interval for the standard deviation divided by $10^{\text{regression intercept}}$ calculated from parameter samples
543 from the Bayesian regression. We see a trend towards much higher variability in posterior
544 spiracle area as compared to anterior. In contrast to spiracle area, spiracle depth shows similar
545 variability in all spiracles (D-F) regardless of position.

Figure 3. Scaling of the spiracles is insufficient to conserve diffusive capacities but more than sufficient to conserve advective capacities in large beetles. (a) The $\log_{10}$ of total spiracular diffusive capacity per beetle (nmol s^{-1} kPa^{-1}) increases with beetle size, but with a slope significantly less than the 0.75 slope of metabolic demand (slope greater than 0.75 in 0 of 10,000 bootstrap replicates). Metabolic rate slope is shown in light grey. (b) The $\log_{10}$ PO_2 gradient (kPa) required to diffusively supply the oxygen demand of beetles increases with beetle size. The upper band shows the range of PO_2 gradients across the spiracles needed for diffusive oxygen supply in flying beetles, while the lower line shows the values for resting beetles at a body temperature of 25°C. The scatter points at the bottom of the flight band represent required PO_2 gradients across the spiracles if metabolic rates during flight are eight times that of rest; the upper scatter points indicate required PO_2 gradients across the spiracles if metabolic rates are ninety times resting values, likely if thorax temperature warms to 40°C and beetles exhibit maximal flight performance. (c) Hypermetric scaling of $\log_{10}$ summed advective capacity (m^3 s^{-1}•kPa^{-1}) versus $\log_{10}$(body mass), showing a decrease in resistance to advective gas exchange in larger insects. The advective capacity scales significantly more steeply than the 0.75 slope of metabolic rate (slope higher than 0.75 in all but 93 out of 10,000 bootstrap replicates). Metabolic rate slope is shown in light grey. Equations of regression lines and R^2 shown for each plot.

563 **Supplemental Materials**

564 Supplemental figure 1. Non-identifiability of phylogenetic signal parameter in pGLS regression
565 model. Left-hand column shows both OLS regression and pGLS regression models plotted for a
566 given spiracle morphology (log of area, depth, area/depth, or area^2/depth) vs log of mass. The
567 Right-hand column shows the log likelihood space for the parameter λ, which scales the off-
568 diagonal covariance terms of the regression model thereby providing an indication of how
569 strongly phylogeny influences the pattern of data distribution. A λ of one indicates strong
570 phylogenetic signal whereas a value of zero indicates no sign of covariance in the data due to
571 phylogeny. The solid red line indicates the maximum likelihood for the parameter used in the
572 model on the left, the dashed red line indicates confidence interval estimates for the parameter
573 value. Note that the log likelihood for the parameter is fairly flat across large section of the
574 possible parameter space, and all confidence intervals on the parameter include zero (no
575 phylogenetic signal). Together, these indicate that many values for λ are similarly likely, and that
576 the strength of the phylogenetic signal is hence non-identifiable (our data does not strongly
577 inform the parameter). Given the weakly-to-non-peaked likelihood distributions, selecting a
578 particular value for λ to use in the model is a largely arbitrary choice, poorly supported by the
579 data.

580

581 Supplementary figure 2. Non-identifiability of the phylogenetic signal parameter as indicated by
582 Bayesian modeling. We constructed a generative model for our data (a multivariate normal
583 distribution with covariance matrix given by the phylogenetic signal) which is analogous to the
584 model assumed in pGLS regression. We included a parameter for λ that scaled the off-diagonal
585 terms of the covariance matrix, analogous to pGLS, and sampled from our model for the various

586 regressions of log spiracle morphology versus log mass. We then plotted the prior for the λ
587 parameter (a beta distribution with shape parameters 1.4 and 1.4) against the samples from HMC
588 sampling. This indicated that the samples for this parameter had no shrinkage: the posterior
589 samples for the parameter matched the prior. This indicates that the data does not inform this
590 parameter, a clear indication that the parameter is entirely non-identifiable given our data.
591 Together, with supplemental figure 1, this indicates that the phylogenetic signal is not
592 informative for our models and does not provide useful information or insight to our analysis.
593
594 Supplementary figure 3. Slopes, intercepts, standard deviations, and quasi-coefficient of
595 variation with confidence intervals generated via non-parametric bootstrapping or Bayesian
596 regression for all spiracles and area, depth, area/depth, or area^2/depth vs mass. All spiracles
597 scaled isometrically. The anterior spiracles are much larger than the posterior ones and hence
598 provide much of the gas exchange capacity for the animal. They also exhibit a much tighter
599 distribution for their area and gas exchange capacity than the posterior ones. The spiracle depth,
600 however, did not show the same level of variation in dimension; all spiracular depths had similar
601 degree of variation. This suggests there may be tighter selective regulation on the morphology of
602 the large spiracles that likely supply the airflow needed for highly metabolically demanding
603 tissue like the flight muscle, legs, and brain.
604
605 Supplementary figure 4. Regression plots for both Bayesian and non-parametric bootstrap
606 analyses. The top set of panels provide results for Bayesian linear regression; the light grey
607 bands provide the 80th and 95th percentile for the posterior predictive distribution for the
608 regression model, the dark grey interval shows the 95th percentile for regression line ranges given

by the slope and intercept samples, the black line the 10th percentile for these regression lines. The bottom panels show regression results from non-parametric bootstrap replicates drawn from the data, with ordinary least squares regression as the summary statistic applied to the subsamples. The grey interval shows the 95th percentile for the regression lines generated by the bootstrap sampling. The repeated light grey lines in both sets of figures indicate the theoretical isometric slope value for the regression of a given morphological trait.

Supplementary table 1. Raw spiracle measurements.

Supplementary table 2. Spiracle measurements in a tidy format.

Supplementary video: Reconstruction of the spiracles and connecting tracheal trunks on one side of the scarab beetle *Dicronorhina derbyana*.

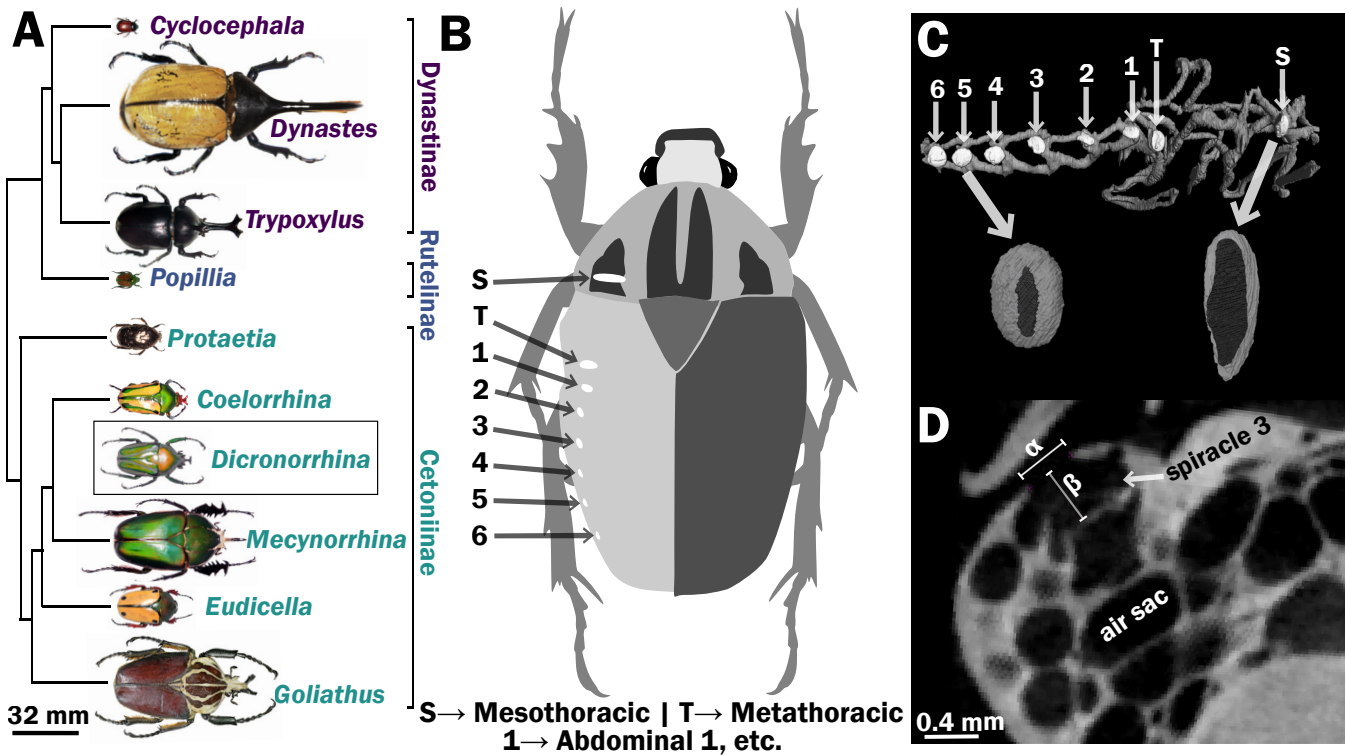
A
Cyclocephala
Dynastes
Trypoxylus
Popillia
Protaetia
Coelorrhina
Dicronorrhina
Mecynorrhina
Eudicella
Goliathus
Dynastinae
Rutelinae
Cetoniinae
32 mm
B
S
T
1
2
3
4
5
6
S→ Mesothoracic | T→ Metathoracic
1→ Abdominal 1, etc.
C
6
5
4
3
2
1
T
S
D
α
β
spiracle 3
air sac
0.4 mm

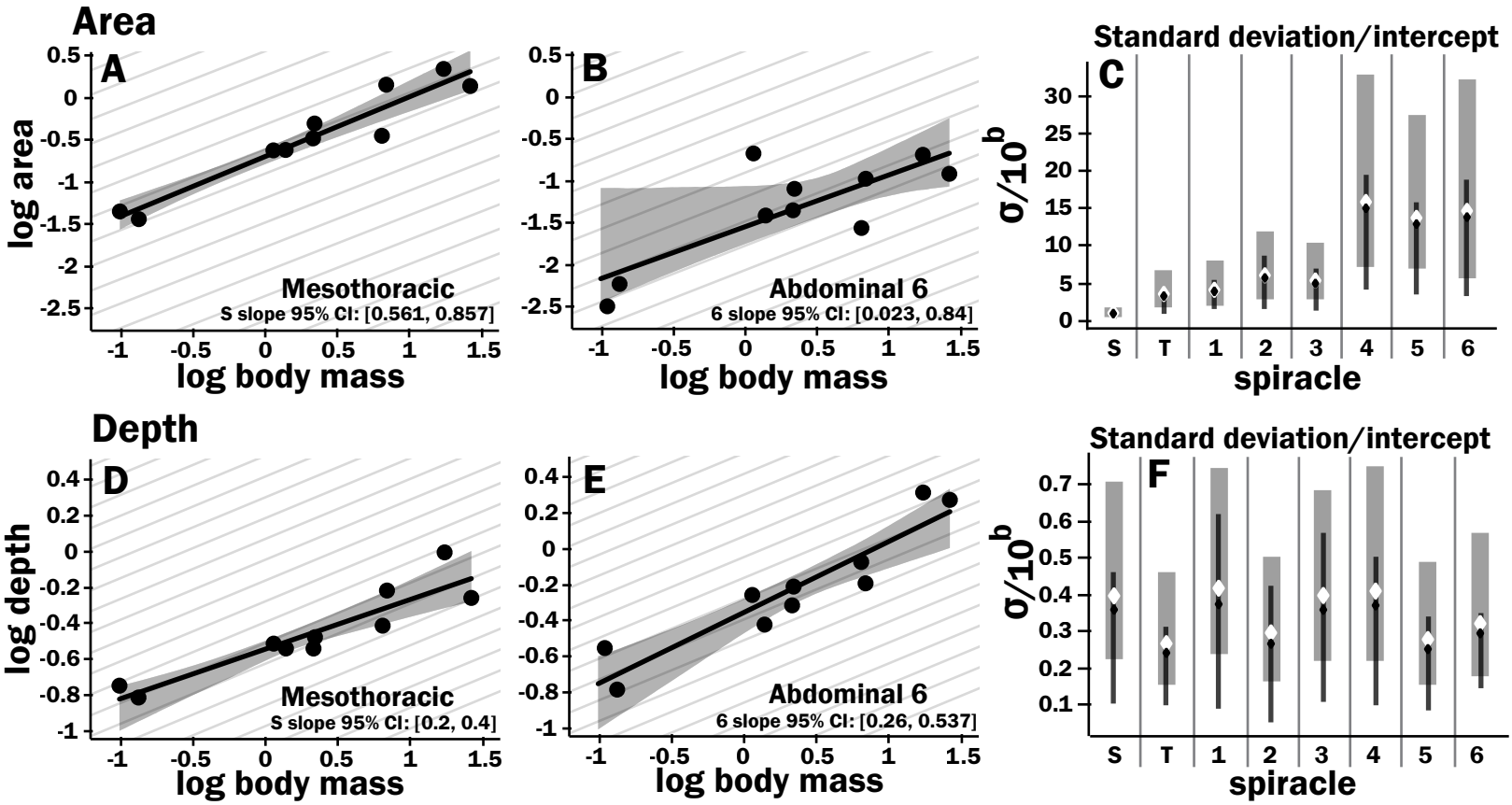
Area
A
log area
Mesothoracic
S slope 95% CI: [0.561, 0.857]
log body mass
B
Abdominal 6
6 slope 95% CI: [0.023, 0.84]
log body mass
Standard deviation/intercept
C
σ/10^b
S
T
1
2
3
4
5
6
spiracle
Depth
D
log depth
Mesothoracic
S slope 95% CI: [0.2, 0.4]
log body mass
E
Abdominal 6
6 slope 95% CI: [0.26, 0.537]
log body mass
Standard deviation/intercept
F
σ/10^b
S
T
1
2
3
4
5
6
spiracle

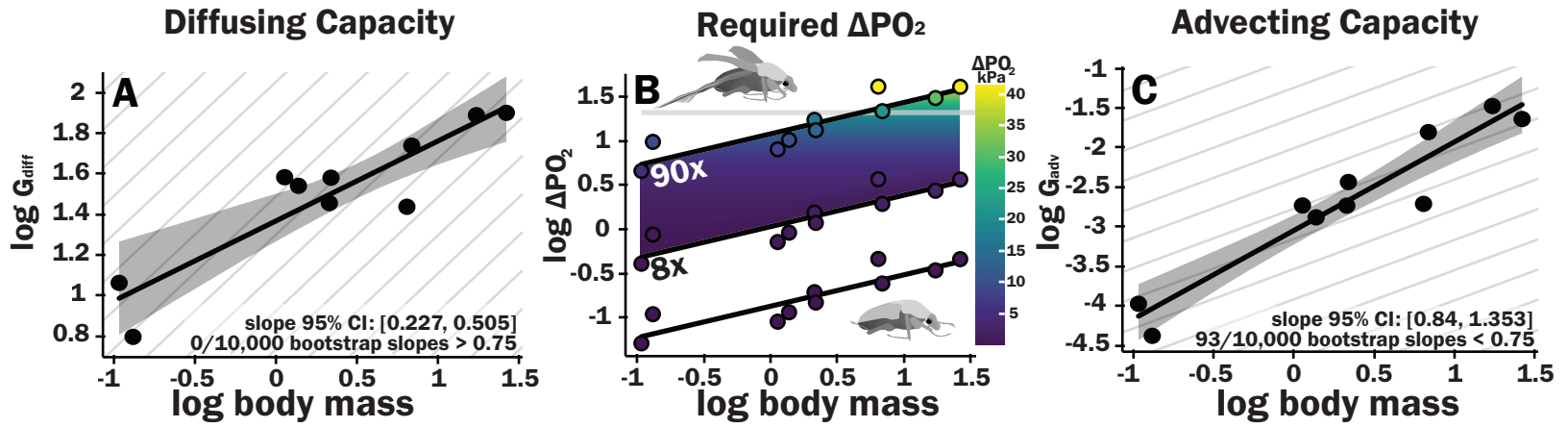
Diffusing Capacity
A
log G_{diff}
slope 95% CI: [0.227, 0.505]
0/10,000 bootstrap slopes > 0.75
log body mass
Required ΔPO_2
B
log ΔPO_2
90x
8x
ΔPO_2 kPa
log body mass
Advecting Capacity
C
log G_{adv}
slope 95% CI: [0.84, 1.353]
93/10,000 bootstrap slopes < 0.75
log body mass

Supplementary Figure 1

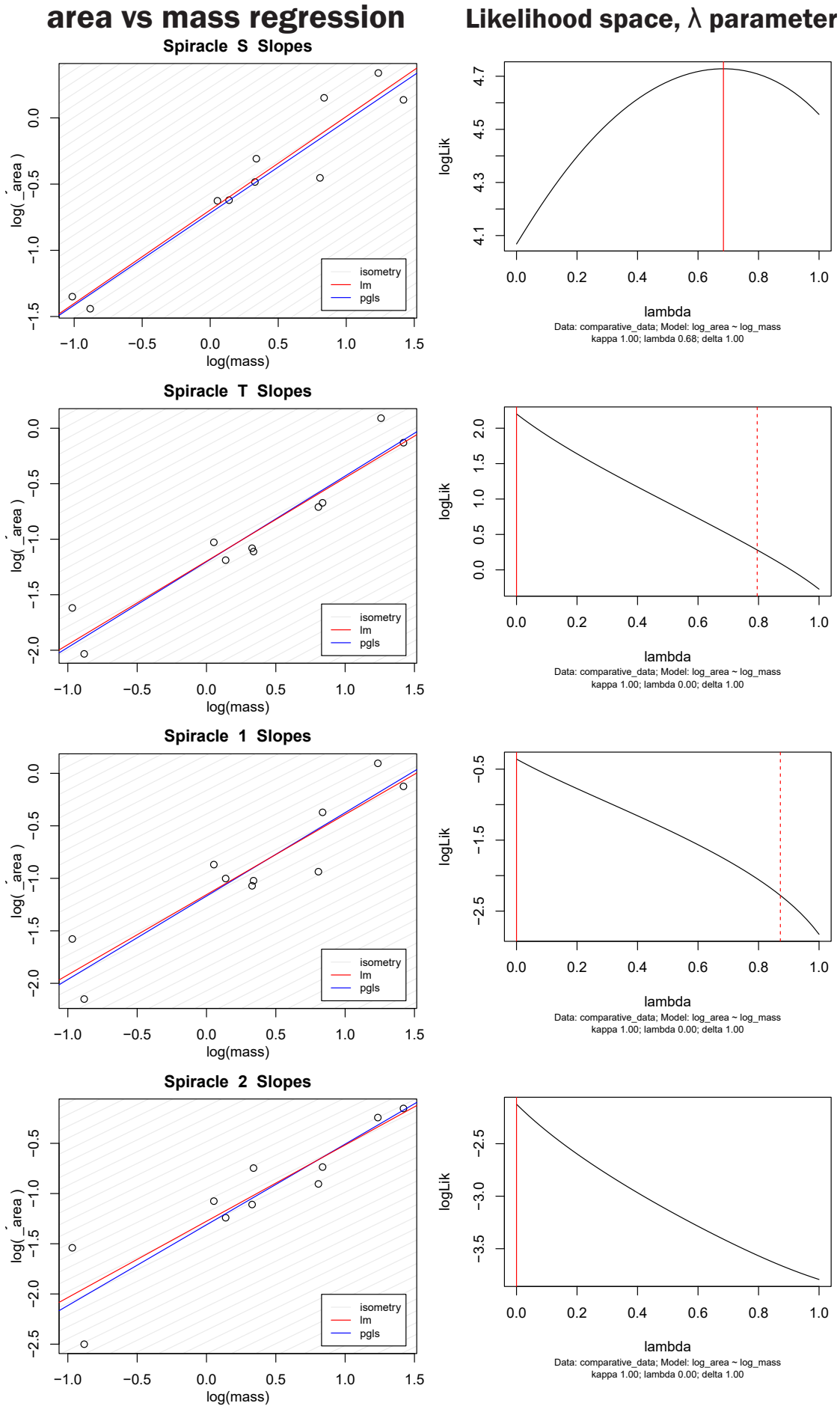

area vs mass regression

Likelihood space, λ parameter

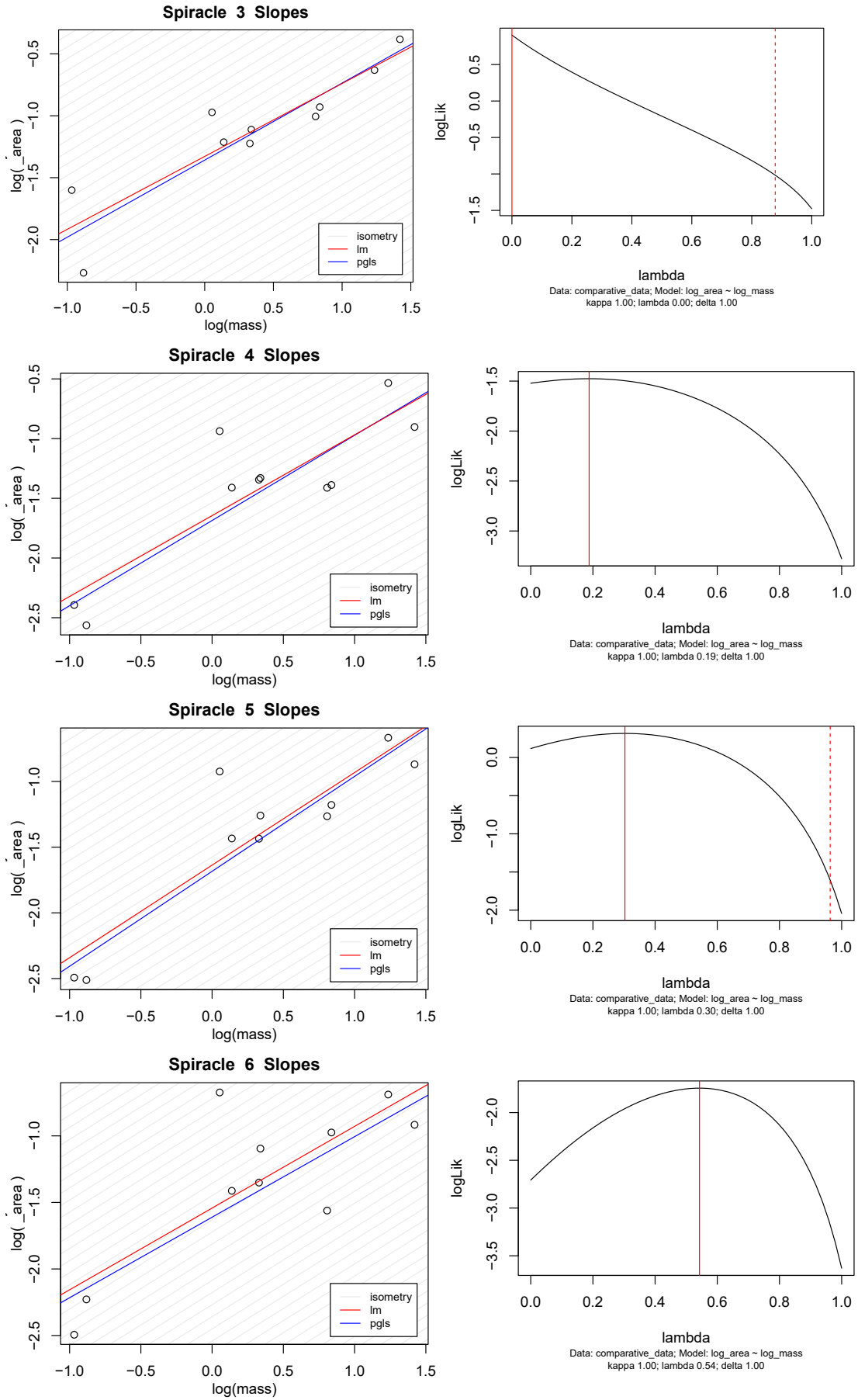

depth vs mass regression

Likelihood space, λ parameter

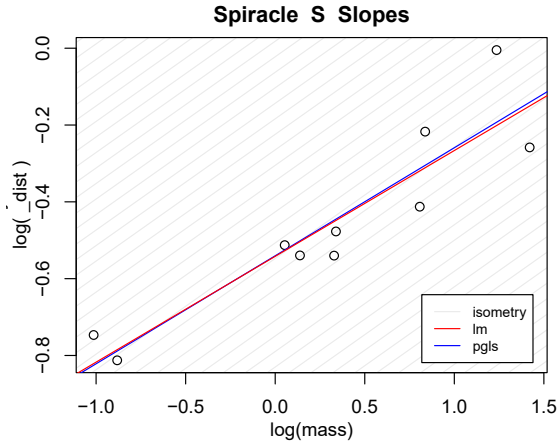

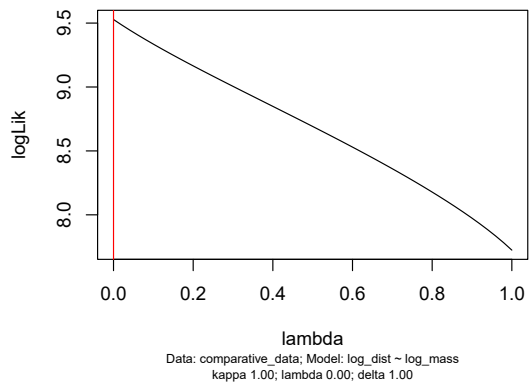

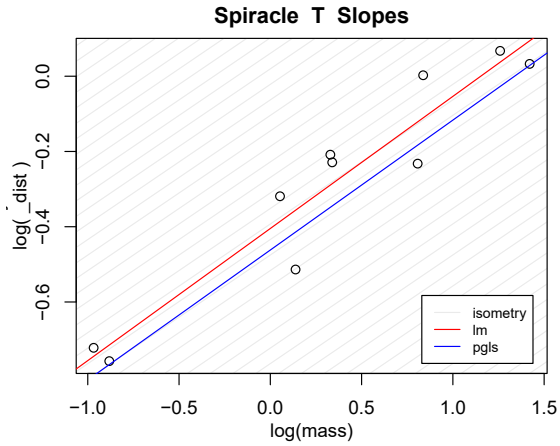

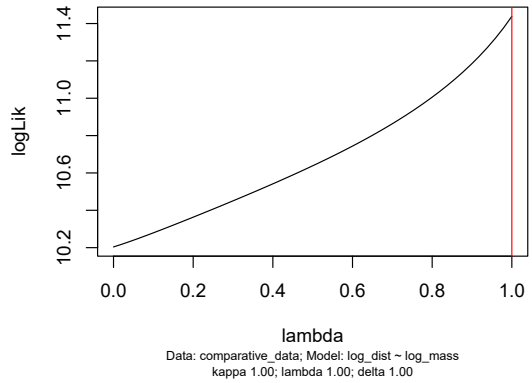

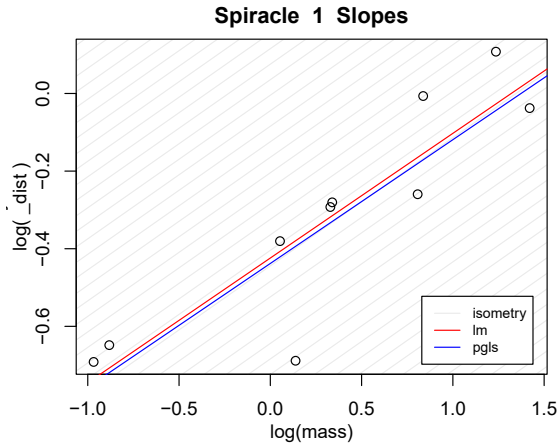

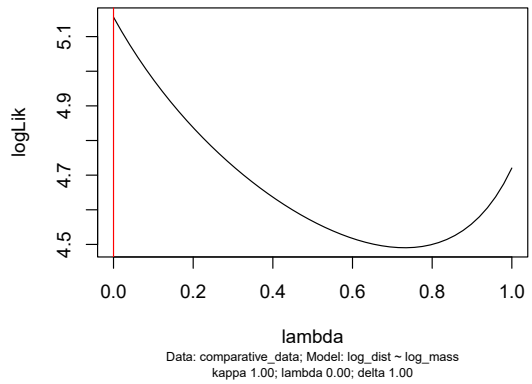

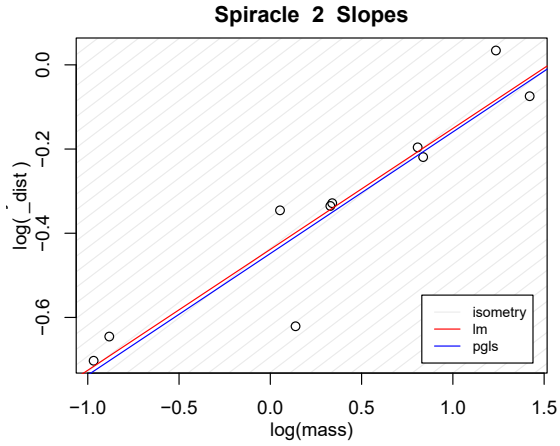

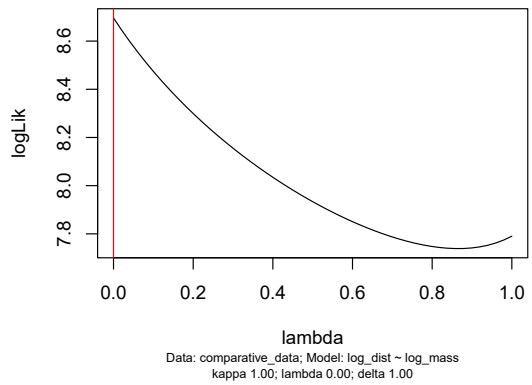

depth vs mass regression

Likelihood space, λ parameter

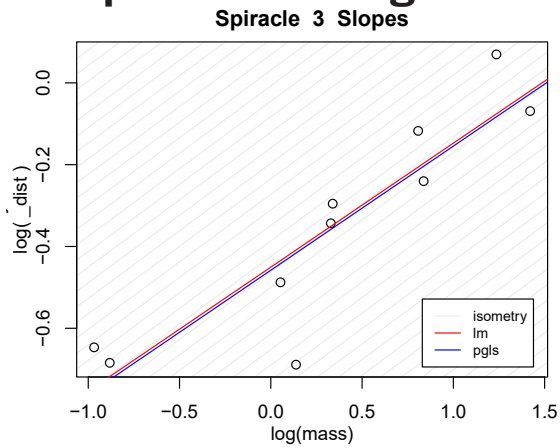

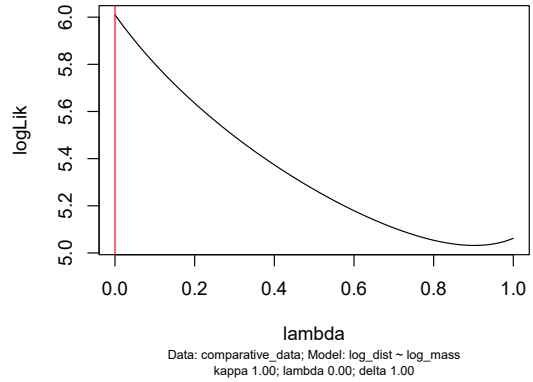

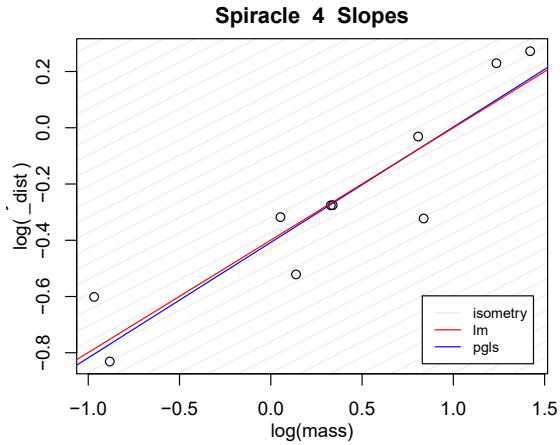

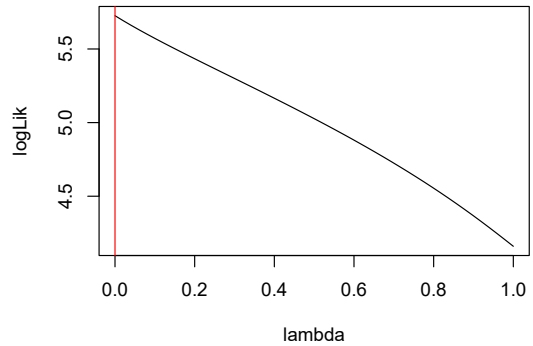

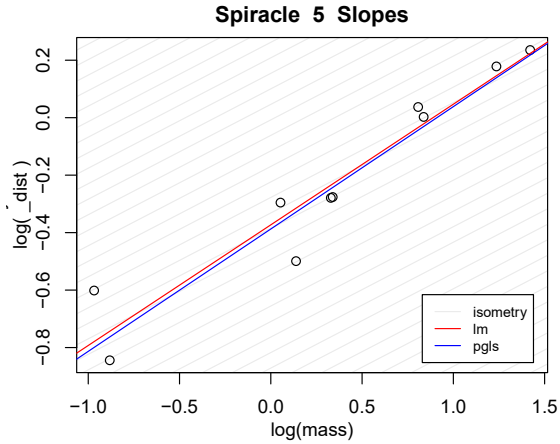

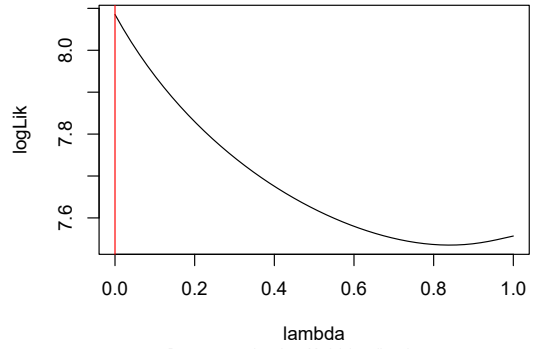

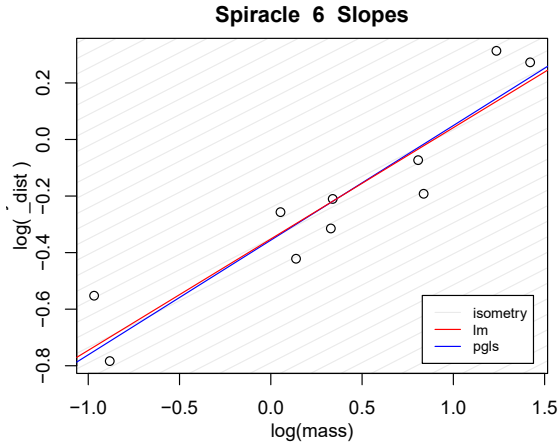

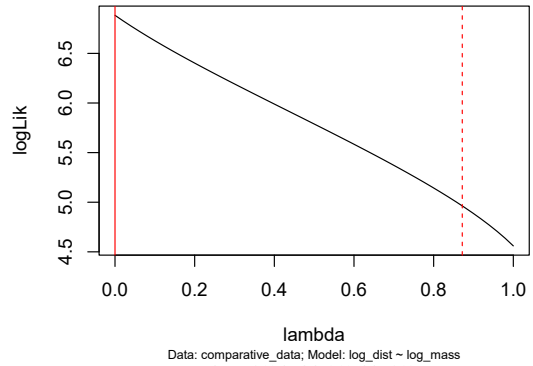

area/depth vs mass regression

Likelihood space, λ parameter

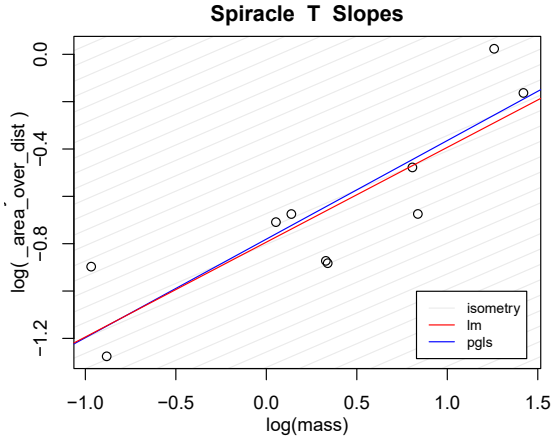

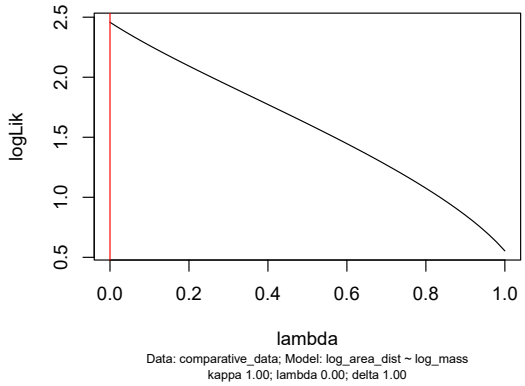

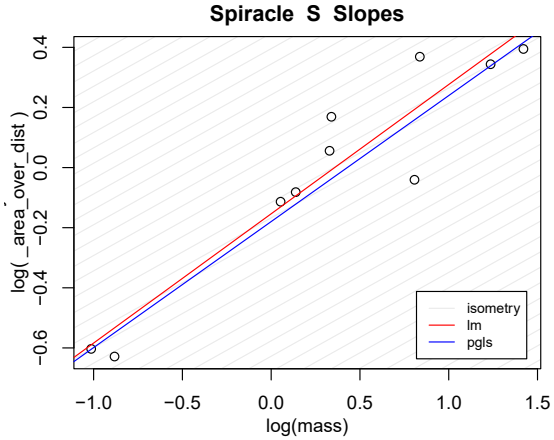

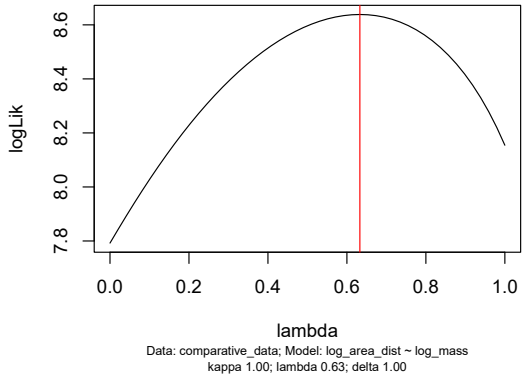

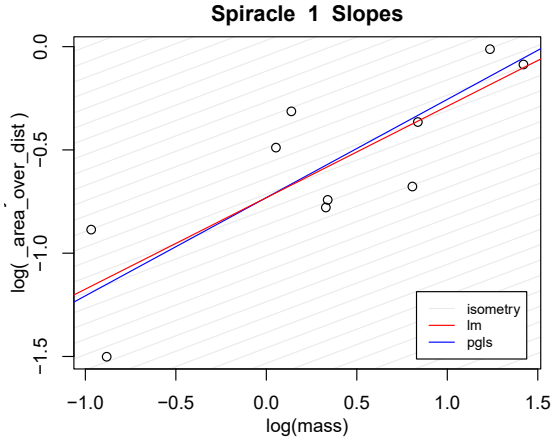

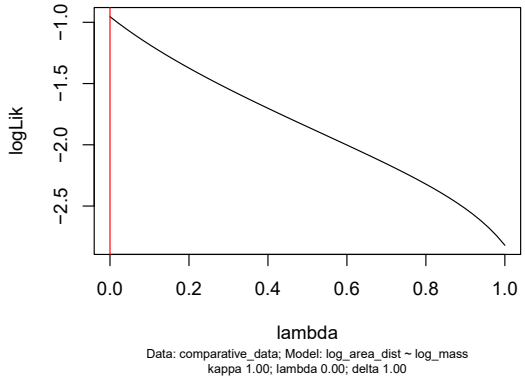

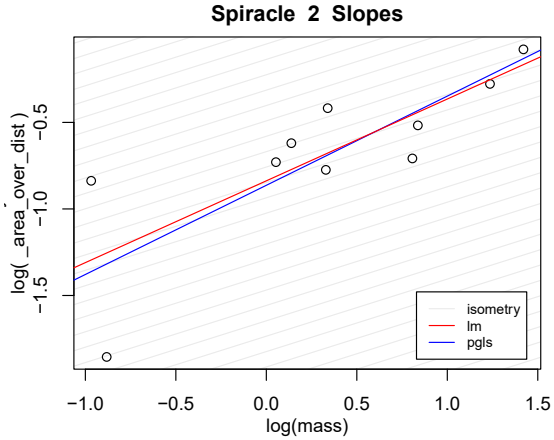

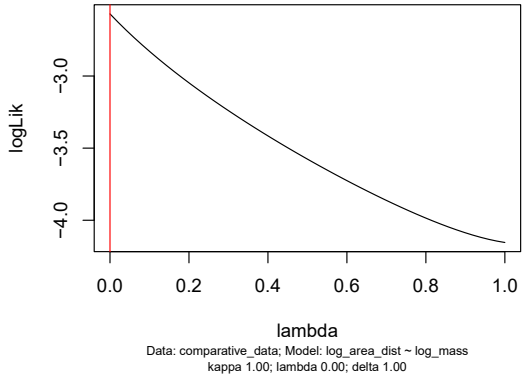

area/depth vs mass regression

Likelihood space, λ parameter

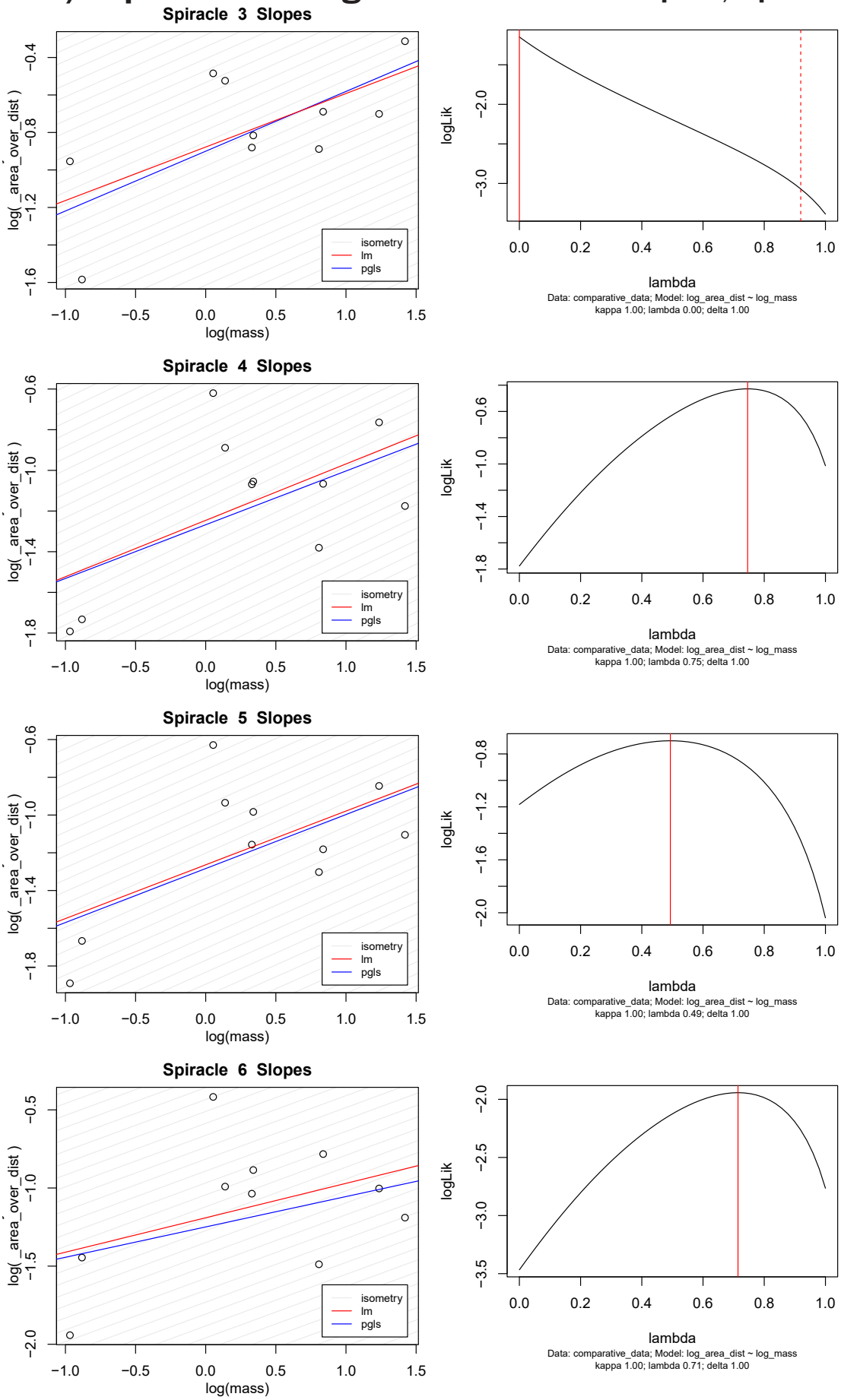

area^2/depth vs mass regression Likelihood space, λ parameter

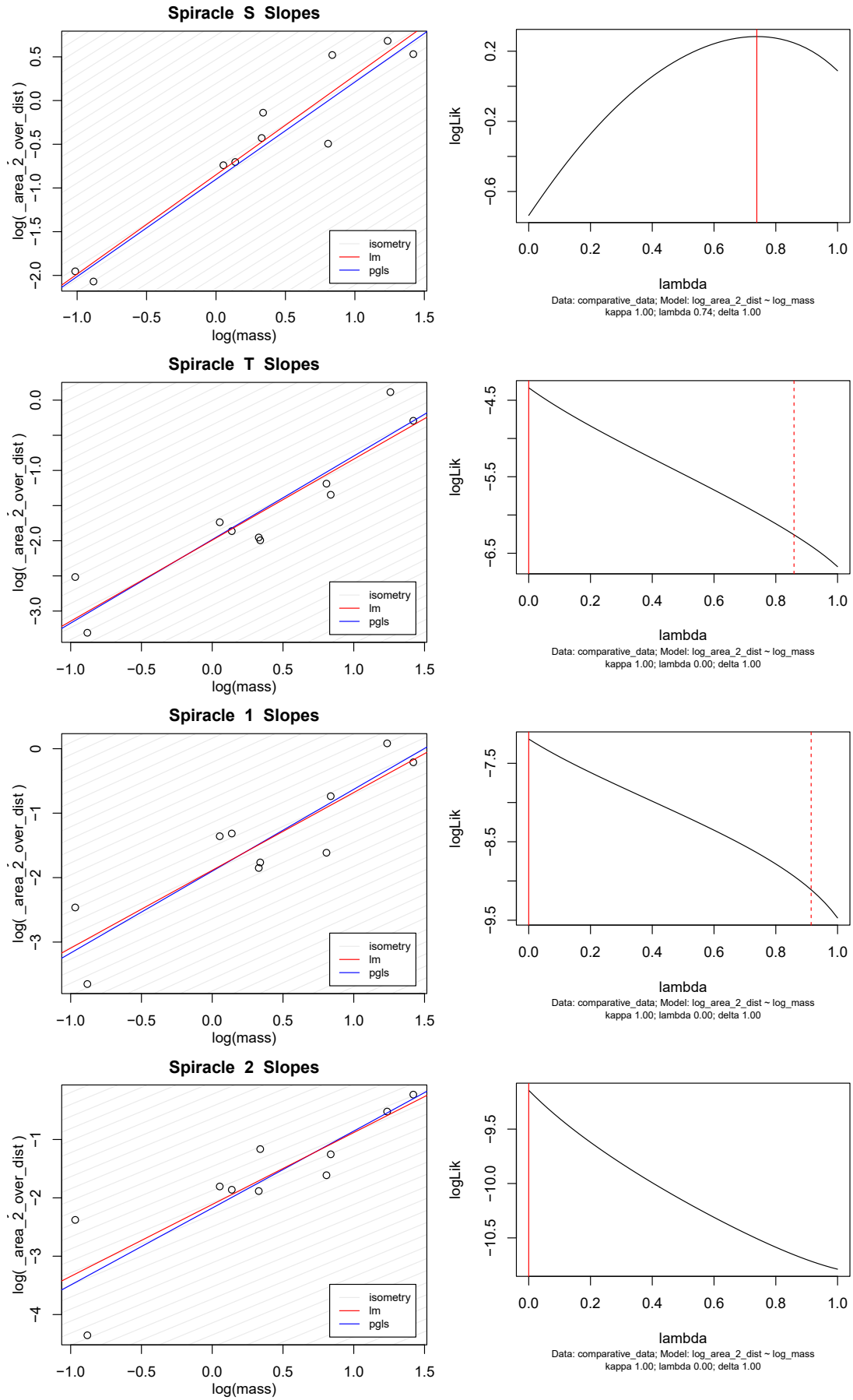

area^2/depth vs mass regression Likelihood space, λ parameter

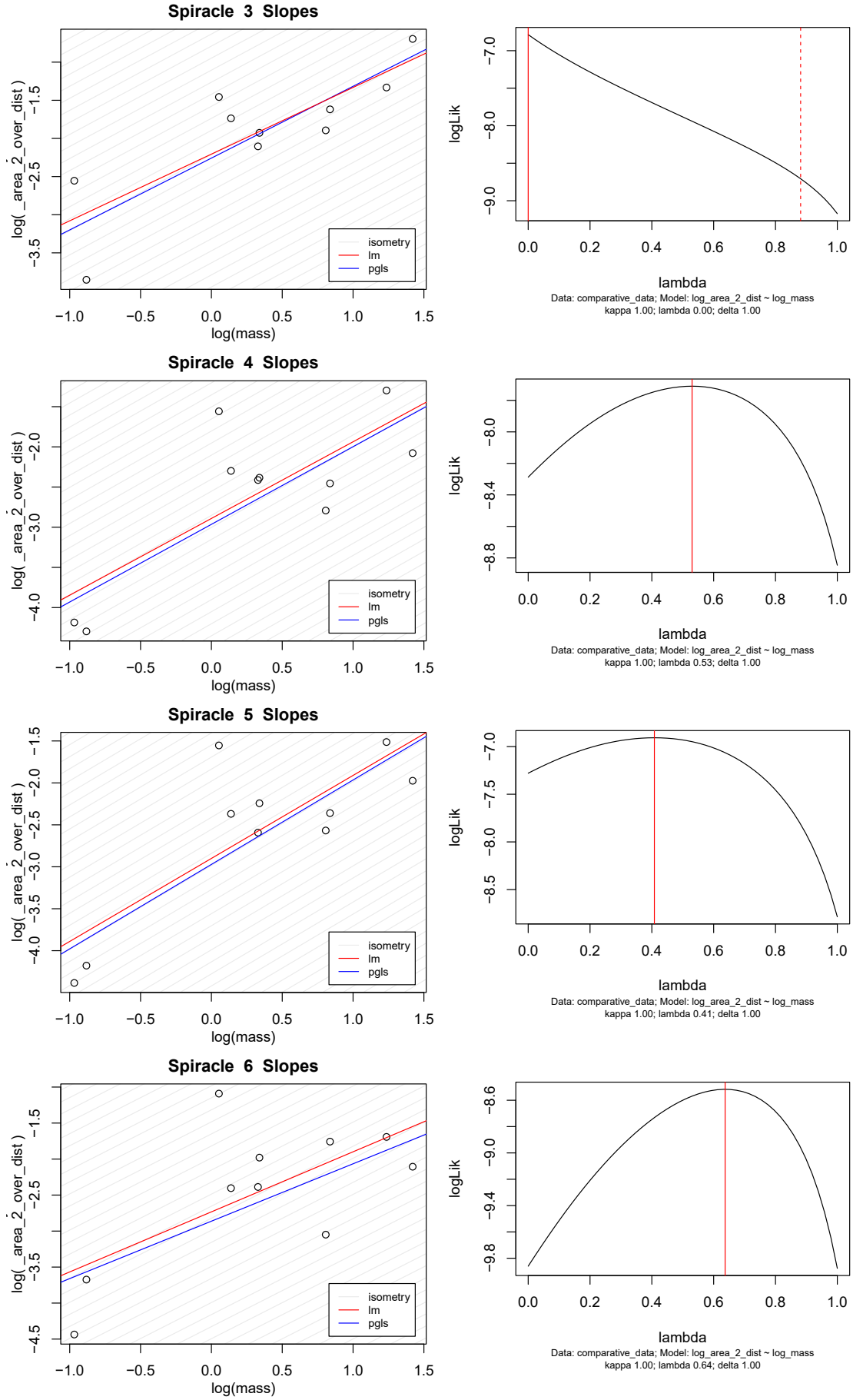

Supplementary Figure 2

Nonidentifiability of phylogenetic signal parameter, area vs mass

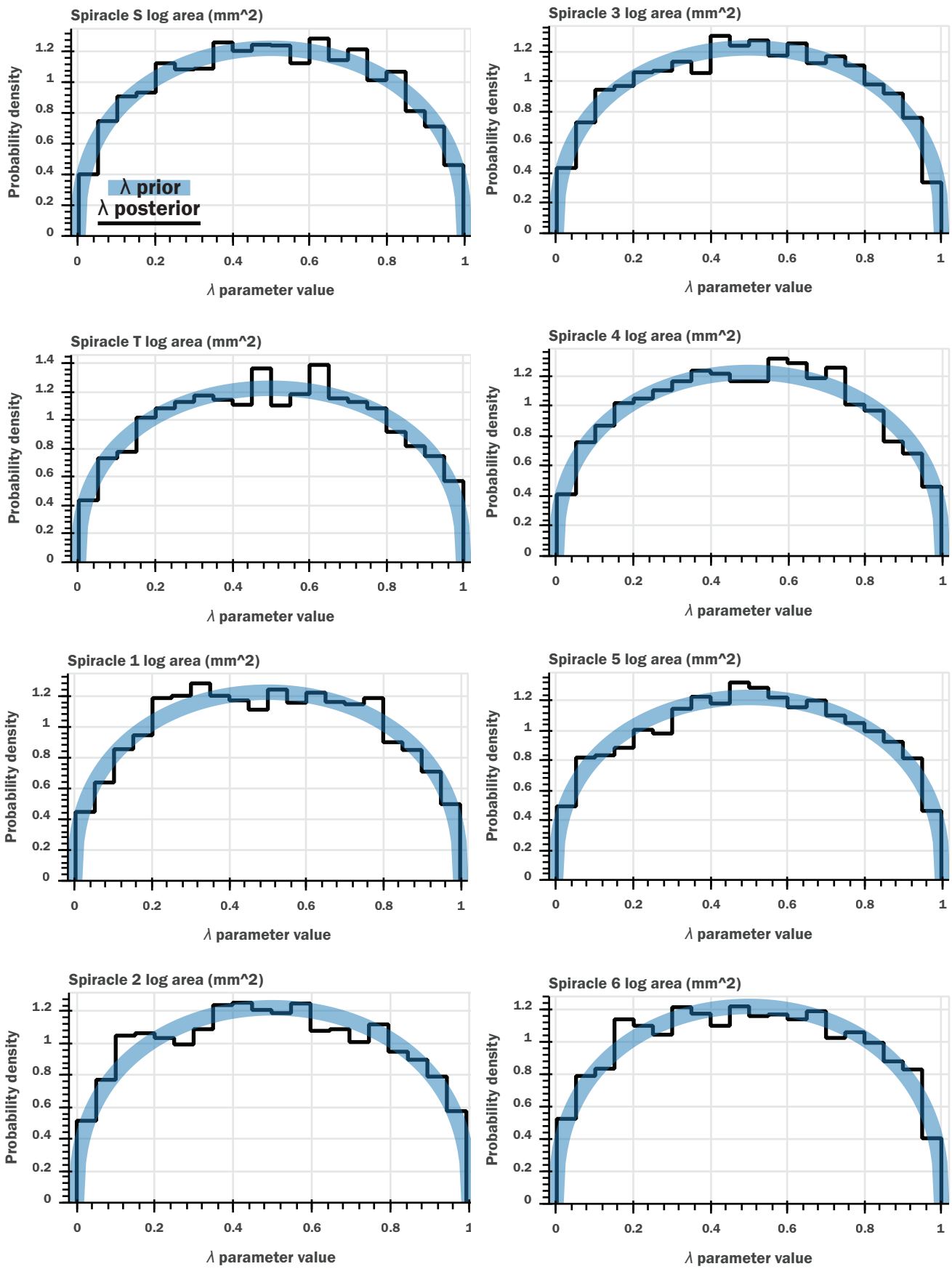

Nonidentifiability of phylogenetic signal parameter, depth vs mass

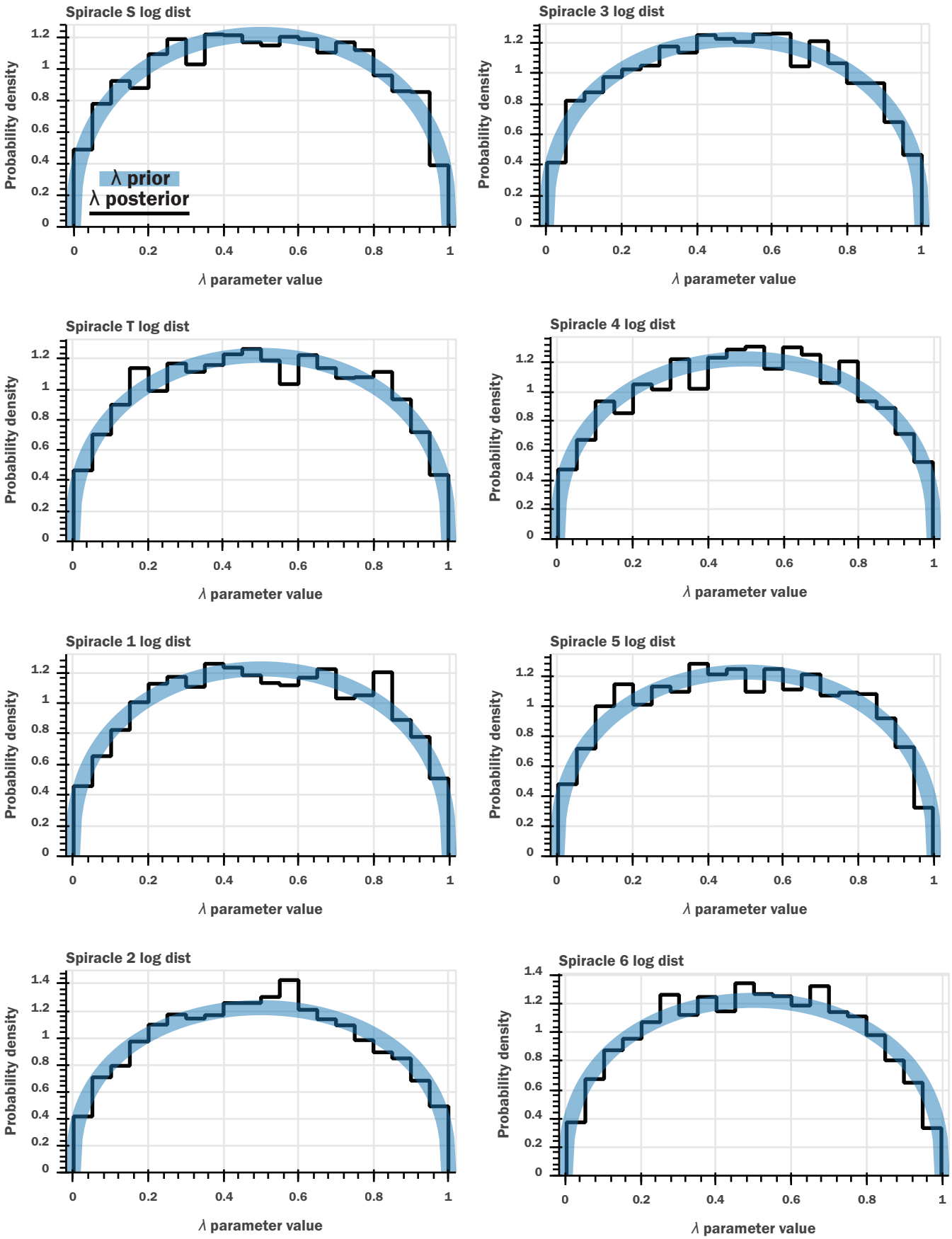

Nonidentifiability of phylogenetic signal parameter, area/depth vs mass

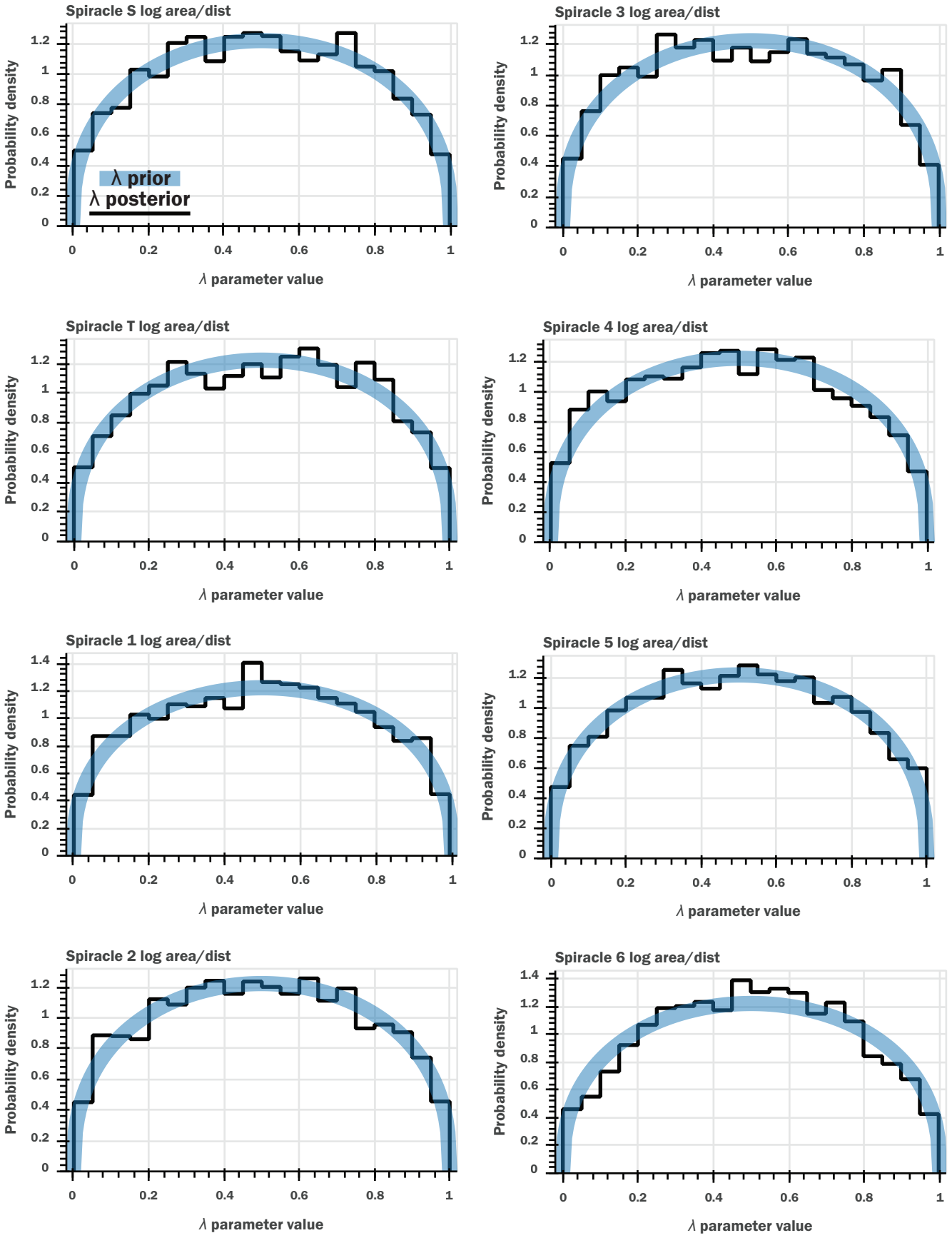

Nonidentifiability of phylogenetic signal parameter, area^2/depth vs mass

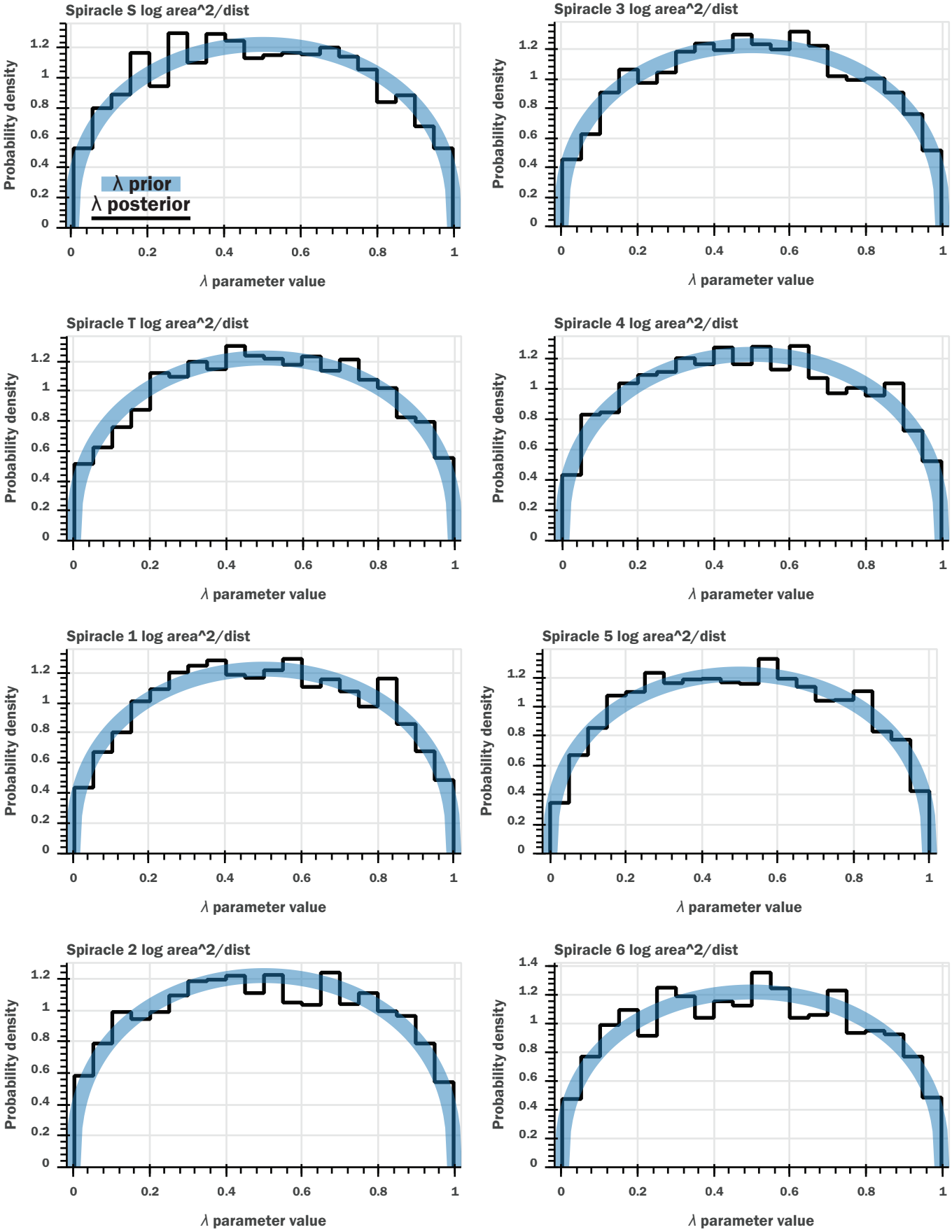

Supplementary Figure 3

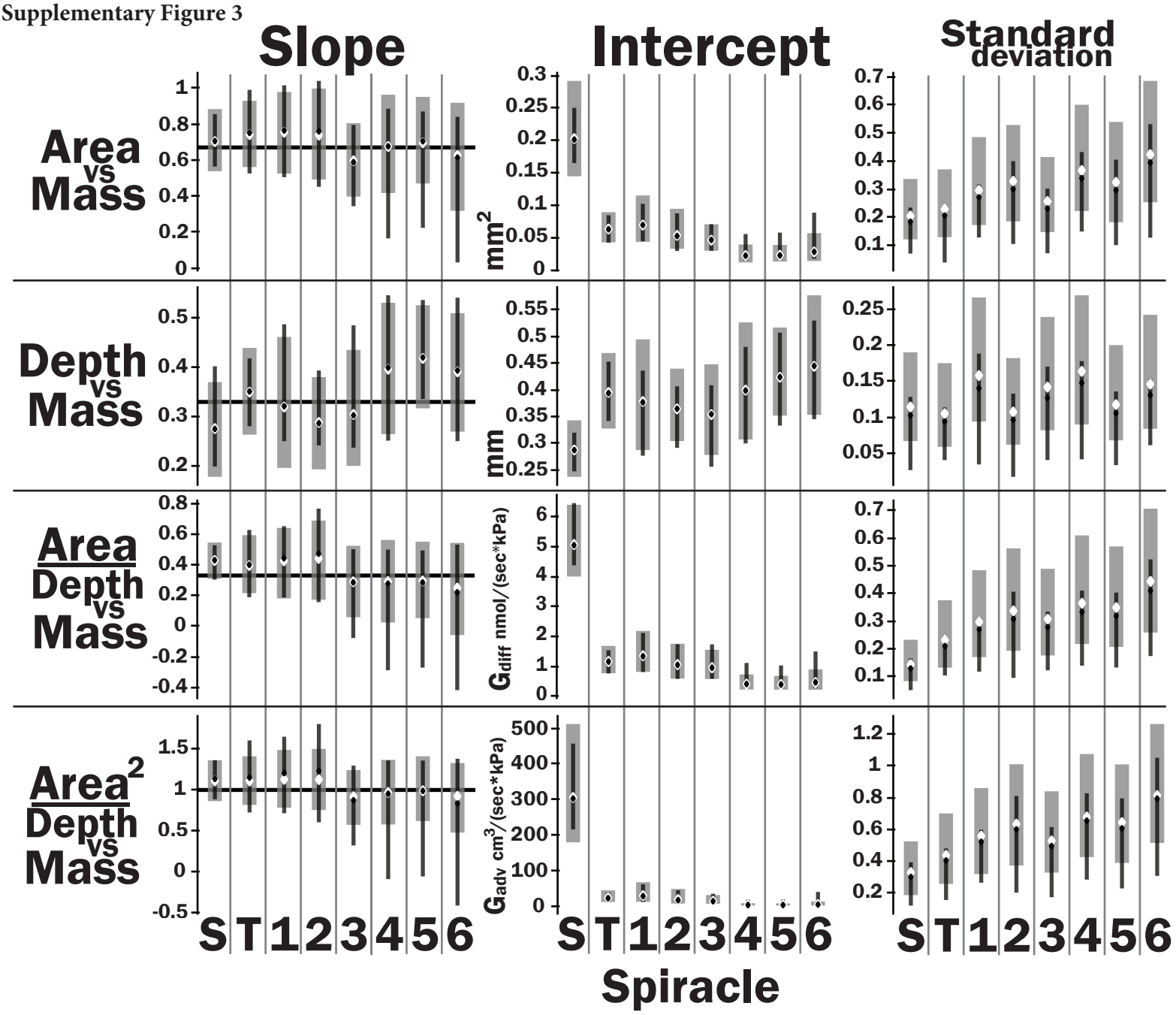

Supplementary Figure 4

Bayesian regression, area vs mass

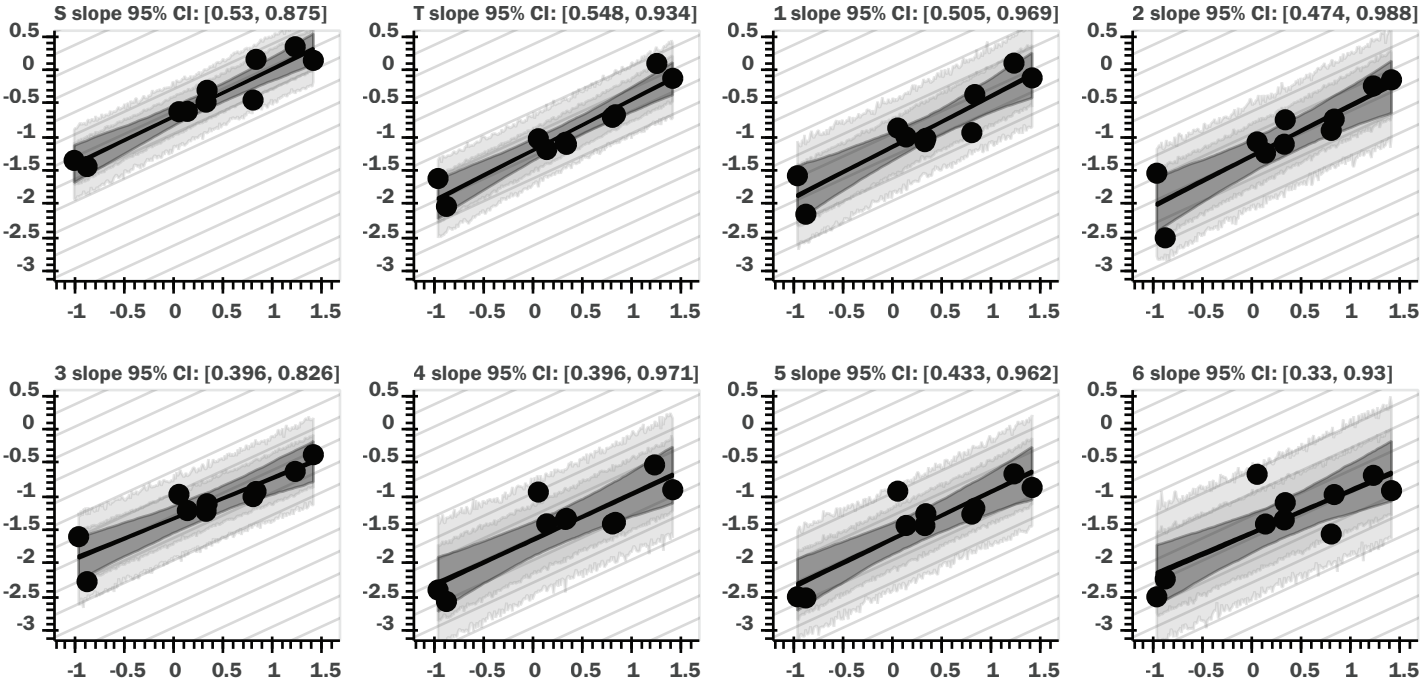

OLS regression, bootstrap CI, area vs mass

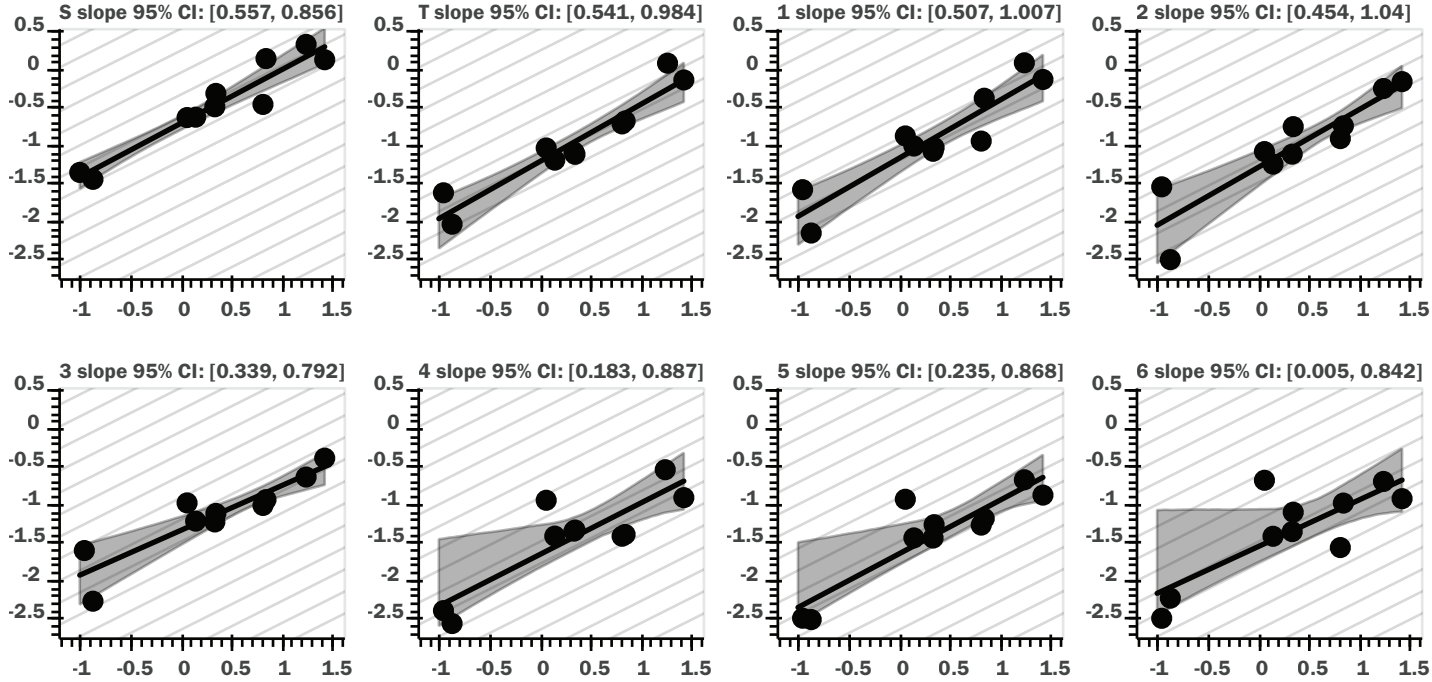

Bayesian regression, depth vs mass

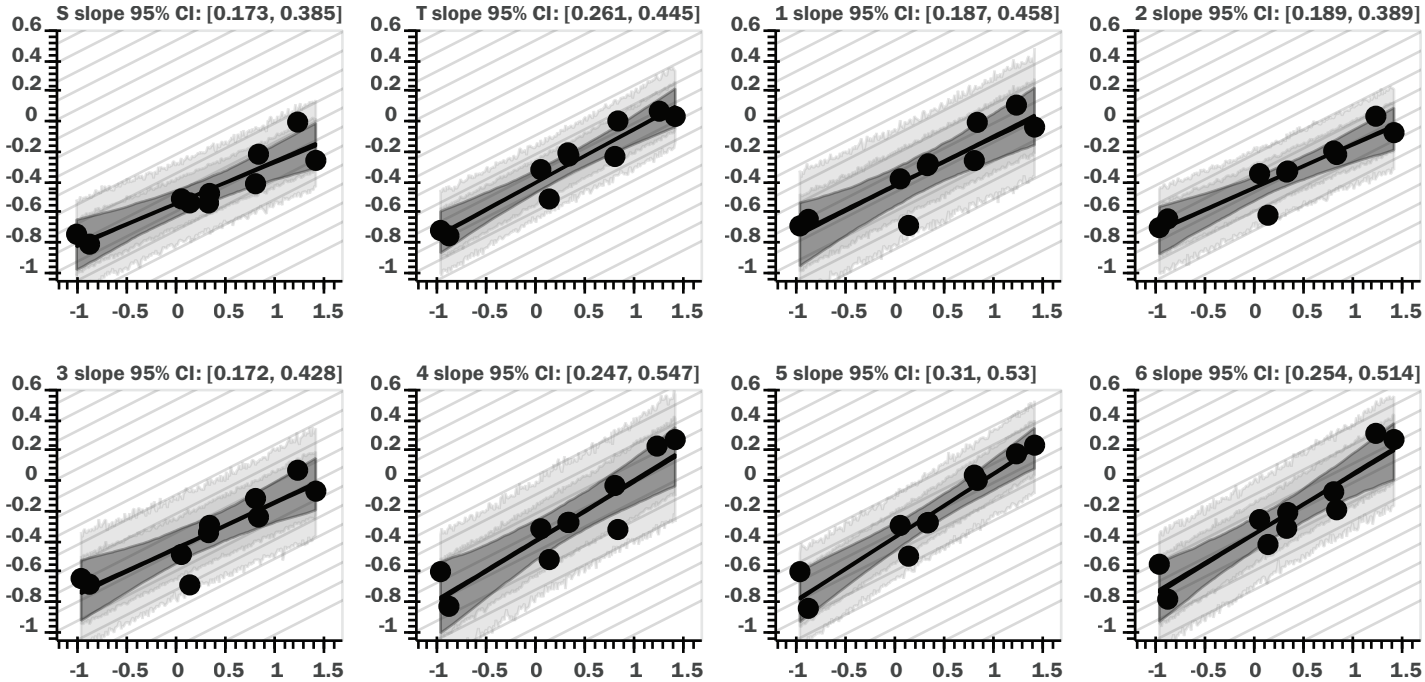

OLS regression, bootstrap CI, depth vs mass

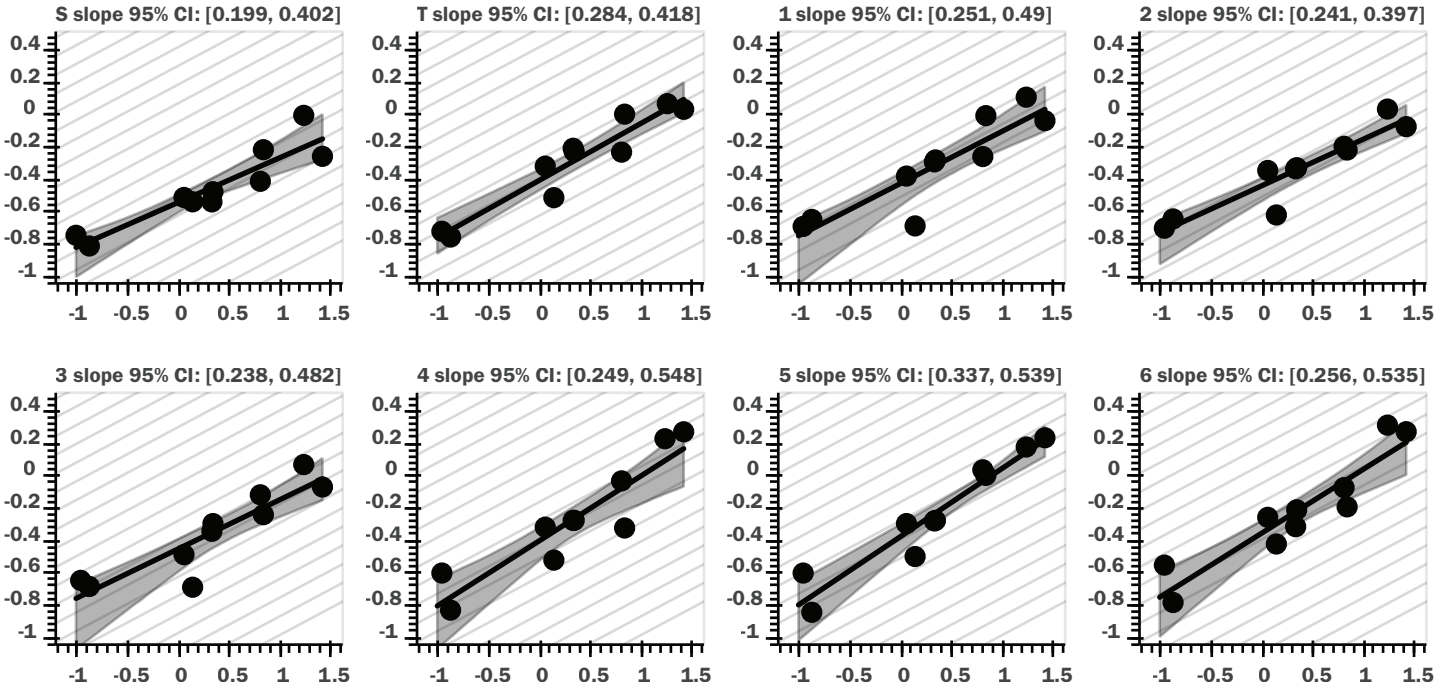

Bayesian regression, area/depth vs mass

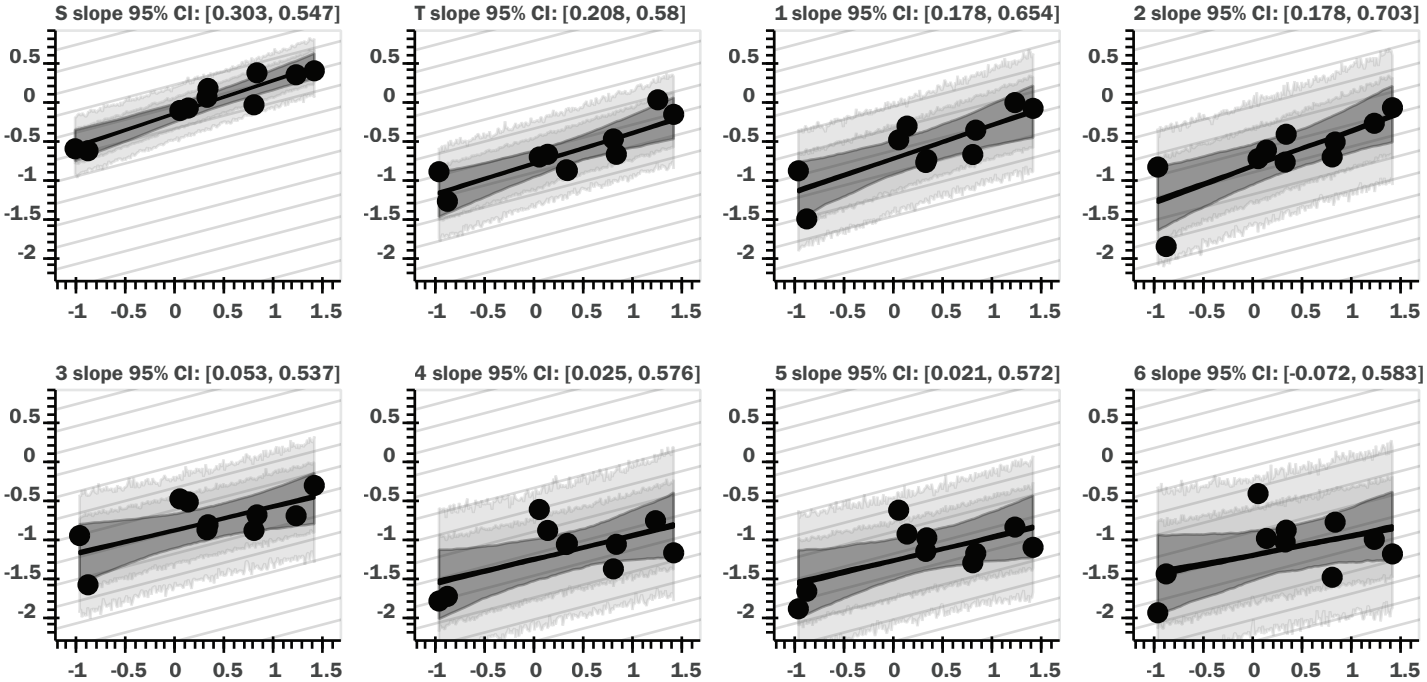

OLS regression, bootstrap CI, area/depth vs mass

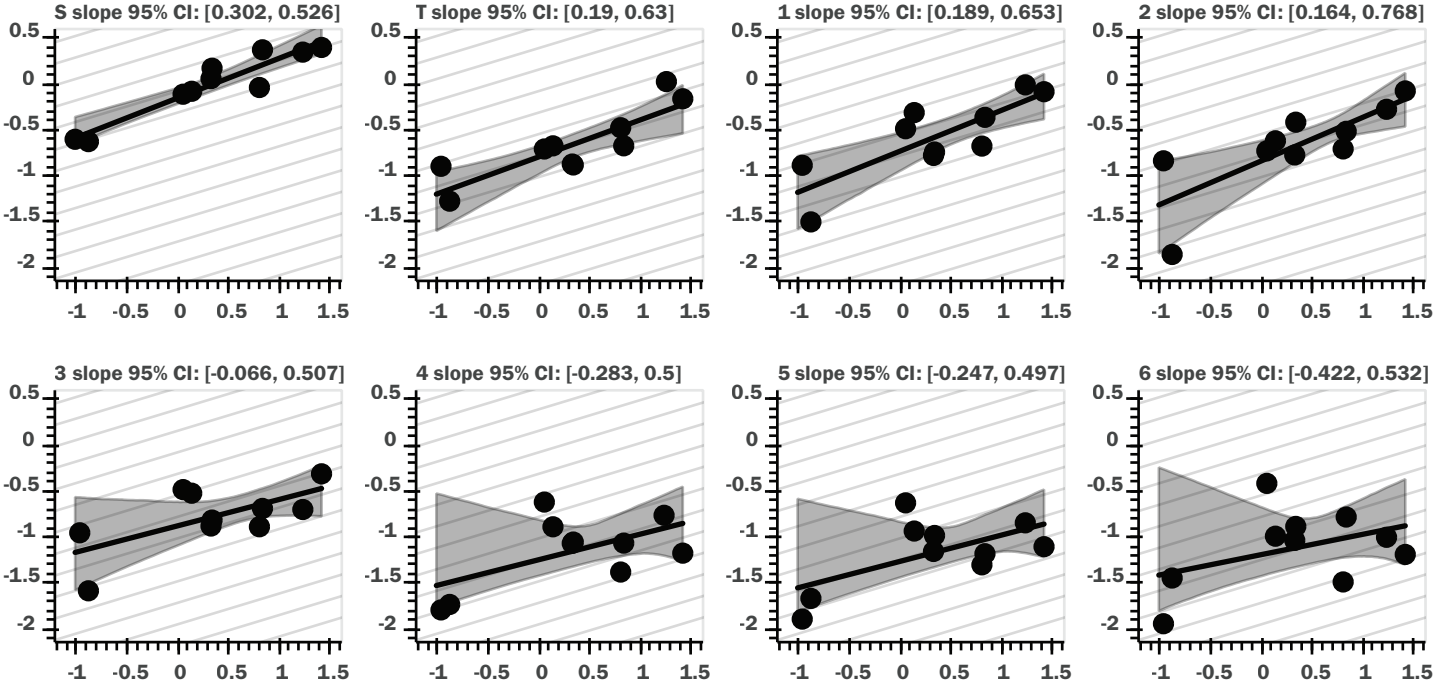

Bayesian regression, area^2/depth vs mass

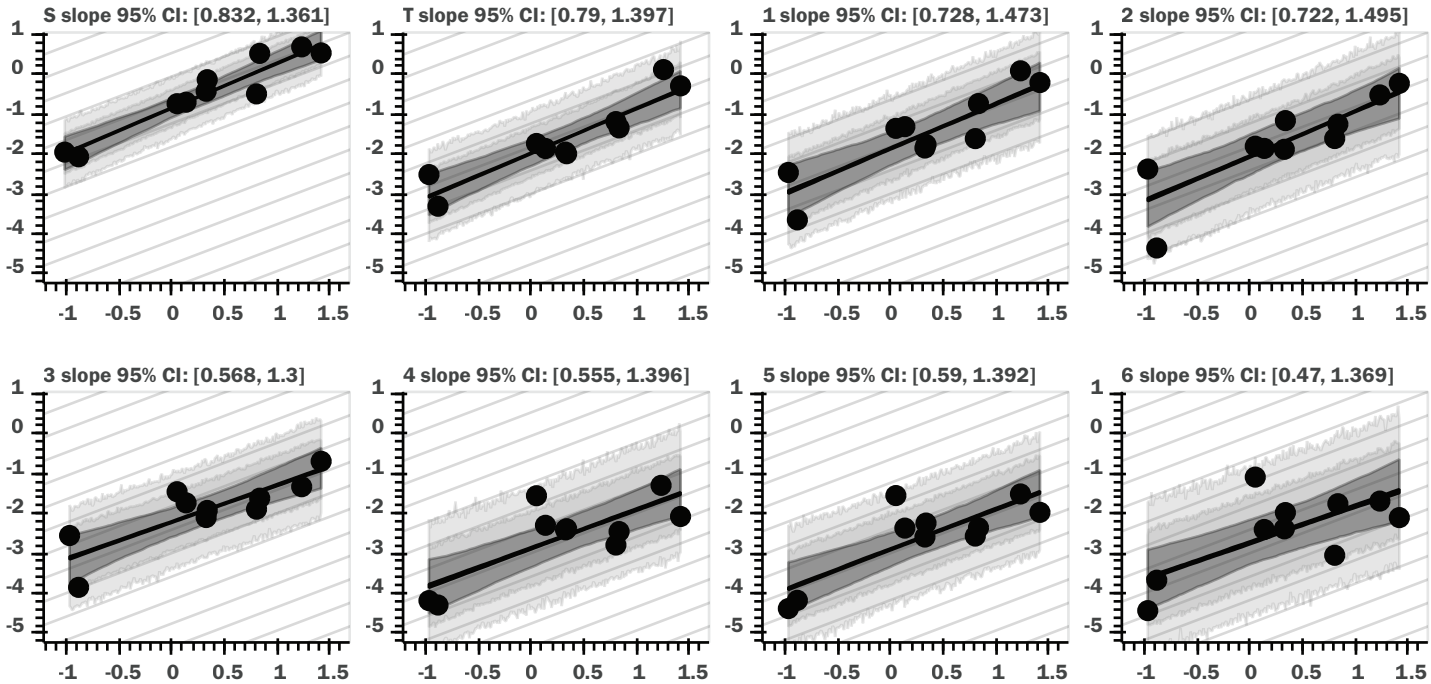
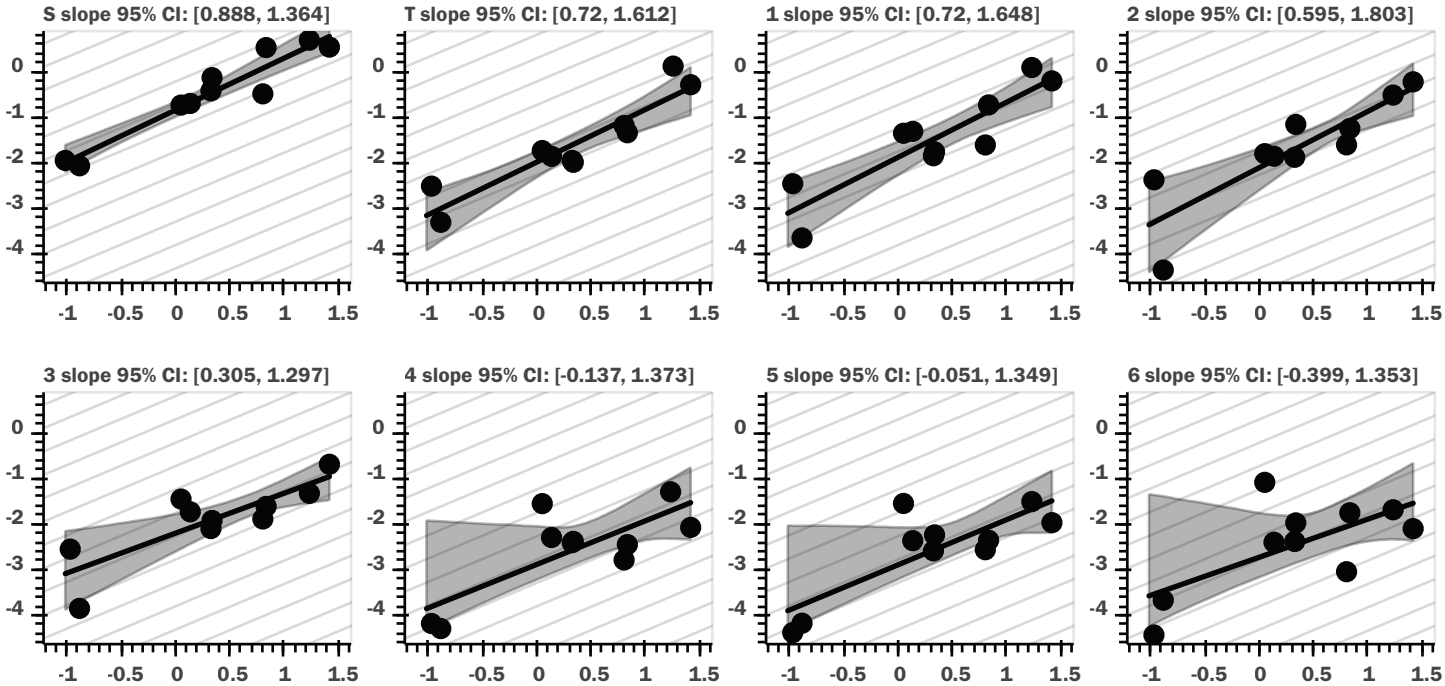
OLS regression, bootstrap CI, area^2/depth vs mass